International Journal of Biological Macromolecules 267 (2024) 131465

Contents lists available at ScienceDirect

International Journal of Biological Macromolecules

journal homepage: www.elsevier.com/locate/ijbiomac

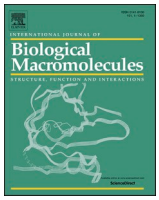

$CdIn_2Se_4$@chitosan heterojunction nanocomposite with ultrahigh photocatalytic activity under sunlight driven photodegradation of organic pollutants

Zaid H. Mahmoud [a,*], Yathrib Ajaj [b], Ali M. Hussein [c], H.N.K. Al-Salman [d], Mohammed Ahmed Mustafa [e], Eftikhaar Hasan Kadhum [f], Sherzod Abdullaev [g,h], Shahad Abdulhadi Khuder [i], Ghadir Kamil Ghadir [j], Safaa Mustafa Hameed [k], Khursheed Muzammil [l], Saiful Islam [m], Ehsan Kianfar [n,*]

[a] Department of Chemistry, College of Sciences, University of Diyala, Iraq
[b] German University of Technology in Oman, Oman
[c] Department of Biomedical Sciences, College of Sciences, Cihan University-Erbil, Kurdistan Region, Iraq
[d] Pharmaceutical Chemistry Department, College of Pharmacy, University of Basrah, Basrah, Iraq
[e] Department of Pharmacy, AL-Nisour University College, Baghdad, Iraq
[f] College of Pharmacy, National University of Science and Technology, Dhi Qar, Iraq
[g] Faculty of Chemical Engineering, New Uzbekistan University, Tashkent, Uzbekistan
[h] Department of Science and Innovation, Tashkent State Pedagogical University Named After Nizami, Tashkent, Uzbekistan
[i] Department of Pharmacy, Al-Hadi University College, Baghdad 10011, Iraq
[j] Al-Farahidi University, College of Pharmacy, Iraq
[k] Department of Optics, College of Health & Medical Technology, Sawa University, Almuthana, Iraq
[l] Department of Public Health, College of Applied Medical Sciences, Khamis Mushait Campus, King Khalid University, Abha, KSA, Saudi Arabia
[m] Civil Engineering Department, College of Engineering, King Khalid University, Abha 61421, Saudi Arabia
[n] Mechanical Engineering Department, Faculty of Engineering and Pure Sciences, Istanbul Medeniyet University, Istanbul, Turkey

ARTICLE INFO

Keywords:
Heterojunction
Photolysis
Nanocomposite
Sunlight
UV-manual system

ABSTRACT

This research focused on synthesizing a $CdIn_2Se_4$@Ch nanocomposite by doping $CdIn_2Se_4$ into chitosan using a photolysis assisted ultrasonic process. The aim was to enhance the photodegradation efficiency of ofloxacin and 2,4-dichlorophenoxyacetic acid under sunlight. The synthesized $CdIn_2Se_4$@Ch nanocomposite was investigated via different techniques, including XRD, XPS, FTIR, TEM, DSC, TGA, UV–Vis and PL. The study also investigated the influence of various reaction parameters, including the effects of inorganic and organic ions. The synthesized nanocomposite demonstrated exceptional efficiency, achieving 86 % and 95 % removal rates, with corresponding rate constants of 0.025 and 0.047 min-1. This performance surpasses that of $CdIn_2Se_4$ by approximately 1.35 and 2.25 times, respectively. The values of COD were decreased to 78 and 86 % for ofloxacin and 2,4-dichlorophenoxyacetic, while the TOC values decreased to 71 and 84 %, respectively, from their premier values. The improvement in performance is associated with the introduction of $CdIn_2Se_4$ into chitosan, resulting in the self-integration of Cd into the catalyst. This creates a localized accumulation point for electrons, enhancing the efficiency of charge separation and further reducing the surface charge of chitosan. Experimental evidence suggests that superoxide and hydroxyl radicals play a significant role in the photodegradation of pollutants. Additionally, the nanocomposite exhibits excellent stability and can be reused up to five times, indicating remarkable stability and reusability of the developed photocatalyst.

1. Introduction

In recent years, a significant amount of chemical substances, such as personal care products, dyes, and organic pollutants, have been released into the environment without proper treatment due to human civilization's advancement [1–5]. The diminishing availability of potable water

* Corresponding authors.
E-mail addresses: zaidhameed_91@yahoo.com (Z.H. Mahmoud), ehsan_kianfar2010@yahoo.com, ehsankianfar775@gmail.com (E. Kianfar).

https://doi.org/10.1016/j.ijbiomac.2024.131465
Received 20 February 2024; Received in revised form 24 March 2024; Accepted 6 April 2024
Available online 9 April 2024

poses a potential global threat to humanity. Furthermore, many of these pollutants are resistant to biological decomposition and persist in the environment [6–9]. Ofloxacin is a pharmaceutical material related with the family of fluoroquinolone and is vastly utilized as antimicrobial compound. The human body cannot completely metabolize fluoroquinolone compounds, with 25–80 % of them being excreted as biologically active compounds [10–12]. Bacteria may undergo genetic changes due to exposure to remnants of antimicrobials present in environmental matrices, leading to the development of drug-resistant bacteria. As a result, these microorganisms require the use of more potent drugs for treating diseases. Additionally, antibiotics are not completely eliminated in wastewater treatment facilities, leading to increased environmental toxicity and bioaccumulation [13–14]. Ofloxacin can persist in aquatic environments and may enter the human body through the food chain or drinking water if pharmaceutical waste and animal waste are not effectively treated. Due to its resistance to biodegradation, it can linger in the environment for extended periods. As a result, conventional methods of removal are limited. It is essential to employ treatment techniques to eliminate the residual antibacterial activity of these compounds. Additionally, 2,4-dichlorophenoxyacetic acid is an organic pollutant that is used as an herbicide to control broadleaf weeds. It is highly toxic and harmful to both humans and animals. Conversely, it shares similarities with the compound Ofloxacin in terms of high chemical stability and low biodegradability, which contributes to its persistent presence in both surface and groundwater. Furthermore, traditional methods such as oxidation, liquid phase adsorption, physicochemical treatment, filtration, coagulation, and biological degradation have been demonstrated to be ineffective in efficiently removing this pollutant [15–17]. Several studies focus on reducing 2,4-dichlorophenoxyacetic acid using reducing agents that contribute to pollution. This approach has various drawbacks, including the requirement for high pressure and temperature [18–20]. Consequently, scholars and scientists are continuously developing techniques to eliminate pollutants from aqueous solutions without generating secondary products, while also achieving high efficiency at a low cost. Advanced oxidation processes have been recognized as an effective method for degrading or mineralizing pollutants and have garnered significant attention due to their affordability and simplicity [21–23]. Recently, there has been an increasing use of advanced oxidation processes (AOPs) that utilize heterogeneous photocatalysts to generate reactive free radicals. These radicals then undergo reactions with pollutants, leading to their degradation in wastewater [24–26]. In general, in AOPs, the generation of photoinduced electron-hole pairs (e–h+) occurs when the photocatalyst is exposed to irradiation with energy that is equal to or greater than its bandgap [27–29]. These pairs engage with adsorbed O_2 and H_2O, initiating a sequence of reactions that result in the formation of reactive oxygen species (free radicals). These free radicals then facilitate the decomposition of harmful waste into smaller products. To enhance the efficiency of this degradation process, it is essential to effectively separate the photoinduced pairs by either transporting charges or through adsorption on the photocatalyst surface [30–31]. This mechanism enables the conversion of severe organic pollutants into smaller, less harmful substances such as carbon dioxide and water. AOP is corroborative as an effective wastewater treatment technology because of its enhanced efficiency of degrading, convenient operating conditions and low cost. The Photo-Fenton-like process is a type of AOP widely utilized for the removal of pollutants [32–35]. Hydrogen peroxide is utilized in the Photo-Fenton-like process to induce the generation of reactive oxygen species, which effectively eliminate organic contaminants in water. Nanomaterials have garnered increased attention as potential agents for wastewater treatment owing to their physicochemical properties, high surface area, and catalytic activity [36–38]. Because of its stability, non-toxicity and low cost-activity, TiO_2 has been used as photocatalyst for different photocatalytic implementation [39–42]. However, its high bandgap value and rapid recombination rate limit its functional applications. Therefore, the development of an improved active photocatalyst in the visible region is necessary for effective utilization of solar irradiation. Various methods such as heterojunction reduction, incorporation, doping, or utilization of supporting compounds for photocatalyst stabilization could reduce the recombination rate of charges and enhance the efficiency of these materials [43–45]. In recent years, there has been significant interest in ternary composites due to their unique catalytic properties. For example, $AgIn_5Se_8$, $ZnIn_2S_4$, $CdIn_2S_4$, etc., have been employed for different photocatalytic implementations [46–48] where $CdIn_2Se_4$ appeared as a good bandgap with 1.87 eV, making it a suitable photocatalyst [49].

Dhruv et al., [22] prepared $Znln_2Se_4$ by hydrothermal method for photocatalytic employment. Chander et al., [23] employed solvothermal to prepare $CdIn_2S_4$ for organic synthesis application. $CdIn_2Se_4$ synthesized through a hydrothermal method was employed for the photocatalytic degradation of dyes in aqueous solutions [24].

Mohammad et al., used Bi_2WO_6-$CoFe_2O_4$ in cefixime removal [25]. Subhiksha et al., employed Ag doped γ-Bi_2O_3 coupled with $CoFe_2O_4$ in ciprofloxacin degradation [26]. Ojo et al., utilized TiO_2-WO_3@GO composite in Oilfield-produced water treatment [27]. Rajeshwari et al., used g-C_3N_4 incorporated α-MoO_3 in p-chlorophenol and rifampicin photodegradation [28]. Kaiqu et al., utilized 2D/2D $Bi_2Fe_4O_9$/$ZnIn_2S_4$ as photocatalyst for degrading antibiotic contaminants [29]. It is synthesized through a hydrothermal process, was employed for the photodegradation of dyes in aqueous solutions. This ternary compound, known as a chalcogenide, exhibits efficient photocatalytic properties. However, its effectiveness is hindered by a high rate of charge recombination, leading to reduced efficiency. To enhance its capability, the incorporation and maintenance of $CdIn_2Se_4$ could be advantageous in inhibiting charge recombination. Additionally, researchers have also developed an integrated approach by maintaining $CdIn_2Se_4$ on the surface of organic compounds for photodegradation applications [50–52]. In this study, a $CdIn_2Se_4$@chitosan nanocomposite has been prepared by a photolysis modified ultrasonic methods for photodegradation of Ofloxacin and 2,4-dichlorophenoxyacetic. The addition of $CdIn_2Se_4$ to chitosan resulted in the formation of a hybrid photocatalyst compound. The synthesized nanocomposite was characterized by utilizing DSC, TEM, XRD, EDX, XPS, DRS and PL. The photoactivity of prepared compounds have been investigated for photodegradation of loxacin and 2,4-dichlorophenoxyacetic under sunlight.

2. Experimental part

2.1. Materials

Indium chloride tetrahydrate ($InCl_3.4H_2O$), selenium chloride ($SeCl_4$), chitosan, oleic acid ($C_{18}H_{34}O_2$), hydrochloric acid (HCl), sodium hydroxide (NaOH), 2,4-dichlorophenoxyacetic ($C_8H_6Cl_2O_3$) and ofloxacin ($C_{18}H_{20}FN_3O_4$) were purchased from Merck Co. and used without future purification. During experiments, de-ionized water was employed in different phases. Despite the focus of photocatalytic studies on ecological applications, the majority of experiments are conducted using pure water. There is a lack of research on how real water samples affect the catalytic degradation of harmful pollutants. Various individual compounds and ions, in addition to water salinity, have been investigated to understand the influence of different components on the photodegradation of pollutants. This was followed by testing the performance in factual H_2O samples such as tap and river water on toxic pollutants such as ofloxacin and 2,4-dichlorophenoxyacetic. Furthermore, the canned mineral H_2O, with a pH 7.02, was bought from nigh store. The systems of local H_2O supported simple arrival to tap water with pH 7.65, while the Khersan river in Iraq's Diyala state served as the sample for the H_2O matrices with pH 8.4.

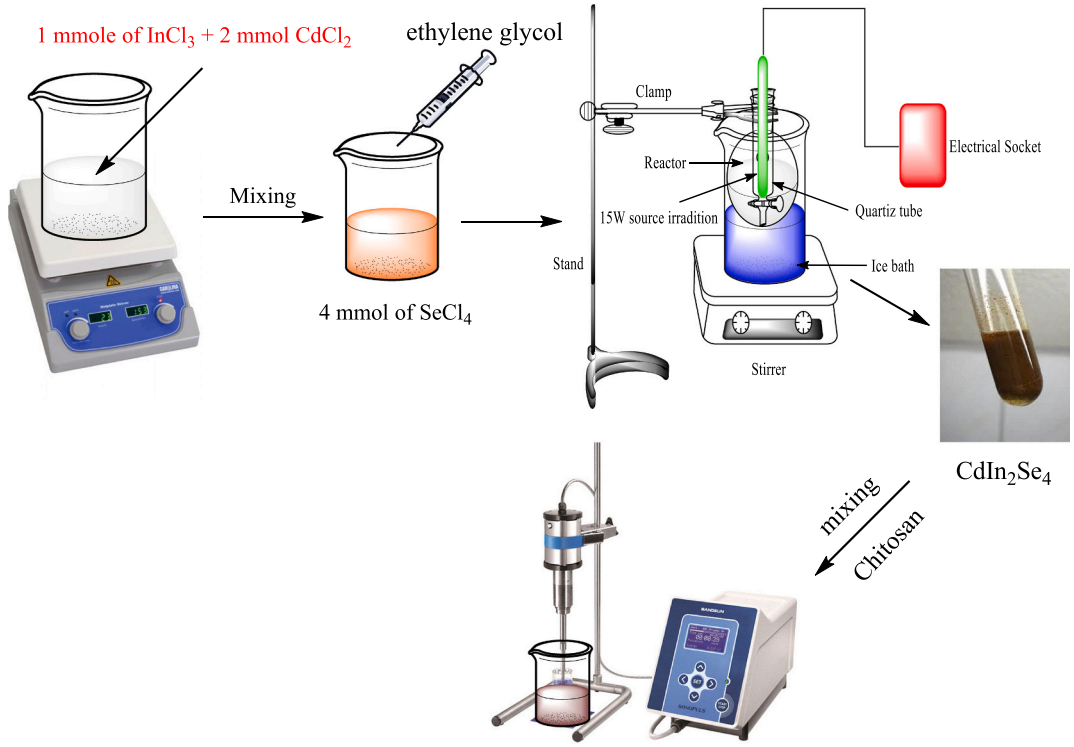

Fig. 1. Schematic process for synthesis of CdIn2Se4@Ch nanocomposite.

2.2. Synthesis of $CdIn_2Se_4$/chitosan nanoparticles

The pure $CdIn_2Se_4$ was synthesized via the photolysis method employing selenium chloride as the selenium source (Fig. 1). 0.2 mmol of $InCl_3.4H_2O$ and 0.1 mmol of $CdCl_2.H_2O$ were combined in 40 ml of ethanol and stirred for 15 min to form Solution A. Solution B was then prepared by adding 0.4 mmol of $SeCl_4$ to ethanol before mixing with Solution A. The resulting mixture was transferred to a manual irradiation system with a power output of 125 W, and the entire procedure was detailed by Zaid et al., [31]. The irradiation process was sustained for 3 h while 3 ml of ethylene glycol was added. The brown precipitate was separated, rinsed, and dried at 60 °C for 2 h, followed by calcination at 550 °C for 3 h. The entire process was repeated prior to subjecting it to ultrasound with chitosan for 30 min at a 1:1 ratio, and then drying it for 3 h at 80 °C.

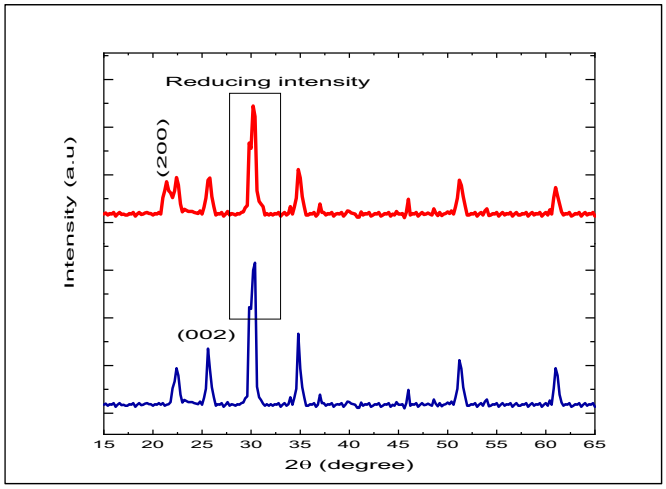

Fig. 2. XRD of pure and $CdIn_2Se_4$@chitosan.

2.3. Photodegradation experimental

The photocatalytic performance of pristine and CdIn2Se4 was examined via oxidative degradation of exemplary pollutant ofloxacin and 2,4-dichlorophenoxyacetic solution with and without H_2O_2. The experiments were conducted in 150 ml beakers with a working capacity of 100 ml, utilizing a 15 W irradiance source emitting light at 365 nm. To maintain a constant temperature in the reactor, circulating cooling water was employed. The experimental setup took place in a wooden room, with an irradiance source positioned at the top of the chamber and the reactor situated at the base, 15 cm away from the light source. Additionally, a magnetic stirrer was used to regulate the speed during the photocatalytic reaction. For this study, 10 mg of photocatalyst was dispersed separately in 100 ml (10 ppm) of ofloxacin and 2,4 dichlorophenoxyacetic acid solution. The dispersion was achieved with magnetic stirring and the mixture was kept in a dark place for 30 min to achieve adsorption-desorption equilibrium. Subsequently, the solution underwent irradiation in 10-min intervals, and 5 ml aliquots of the suspension were withdrawn and their absorption at specific wavelengths was measured. The experiments were conducted under optimized conditions including H_2O_2 concentration, pH level, catalyst dosage, and pollutant concentration for both ofloxacin and 2,4-dichlorophenoxyacetic acid at room temperature. An adsorption state of approximately 2 % was observed for the contaminant, which was considered negligible in all experiments. The chemical oxygen demand (COD) was investigated employing traditional method. For solution including H_2O_2, an excess 7 % Na_2SO_3 was appended, and the mixture was heated to oxidize additional to limit peroxide hydrogen intervention in COD experiments [32]. The efficiency of photodegradation was defined via the following equation (Eq.1):

$$\eta = \frac{C_o - C_t}{C_o} \quad (1)$$

where Co: initial concentration, Ct: the concentration of pollutants at different time. On the other hand, the photocatalytic process kinetic is determined according to the following equation (Eq.2):

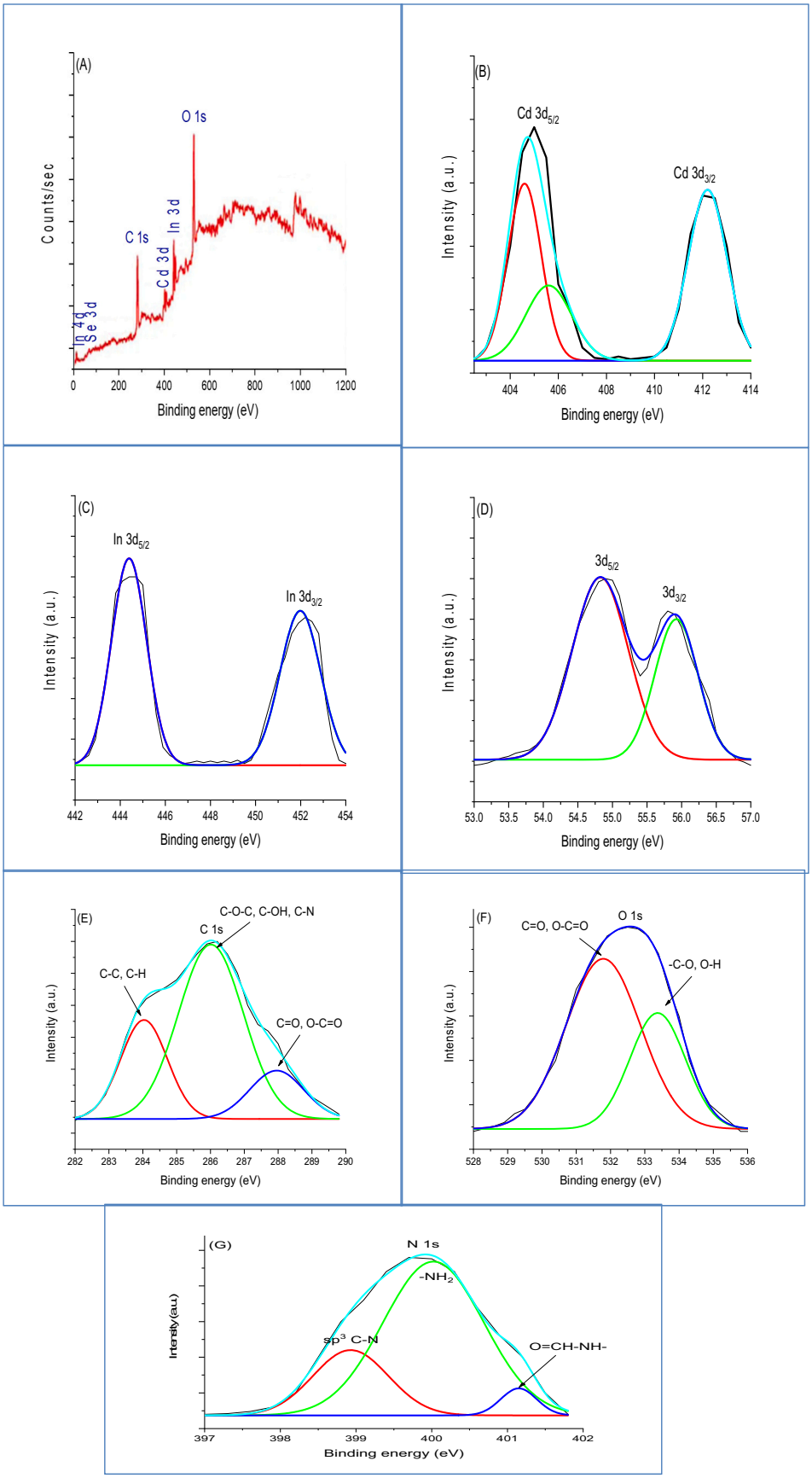

Fig. 3. XPS spectrum of CdIn2Se4@Ch nanocomposite (a) survey spectrum, (b) Cd 3d, (c) In 3d, (d) Se 3d (e) C 1 s, (f)) 1 s and (g) N 1 s.

Table 1
chemical parameter of synthesized photocatalyst.

Sample	2θ	D nm	Metal	Peak BE	FWHM eV	Area (P) CPS.eV	Atomic %
$CdIn_2Se_4$	30.23	12	Cd	405.23	2.25	64,480	11.86
			In	444.23	3.20	76,470	14.24
			Se	54.83	3.35	108,070	19.88
$CdIn_2Se_4$@Ch	30.39	10	C	284.05	4.65	136,770	25.13
			O	531.82	4.10	160,108	29.51

$$ln\frac{Co}{Ct} = Kt \tag{2}$$

where k: constant of reaction rate. The mention two equations were used to calculate quantum yield and figure of Merit (FOM) [33] from following equation (Eq.3 and 4):

$$\Phi = \frac{decay\ rate}{Photon\ Flux} \tag{3}$$

$$FOM = \frac{conversion\ energy\ (\%)}{m\ (g)*Co\ (ppm)*t(min)*P\ (W)} \tag{4}$$

3. Results and discussion

3.1. Structure characterization

Fig. 2 demonstrates the XRD results obtained to assay the $CdIn_2Se_4$ and $CdIn_2Se_4$@Chitosan crystal structure respectively. The diffraction peaks and corresponded Millar indices for pure and $CdIn_2Se_4$@chitosan nanocomposite are in agreement with (**JCPDS: 08–267**). However, in the synthesized $CdIn_2Se_4$@Chitosan nanocomposite, a little shift in the diffraction peaks was revealed because of the chitosan in the $CdIn_2Se_4$ [34]. Conversely, the change might be connected to the modification in particle size and the interaction between chitosan and CdIn2Se4. Moreover, when CdIn2Se4 was treated with chitosan, a rearrangement of the lattice occurred, leading to conflicting stress and resulting in a red shift of peaks. The findings revealed the emergence of a new diffraction peak at 20.21 (220), corresponding to chitosan in the fabricated nanocomposite [34,53–55]. After the synthesis of a photocatalyst nanocomposite, the intensities of some peaks were observed to change, while others decreased due to the incorporation of chitosan, resulting in an alteration in the electron density of atoms [35]. The crystallite size of pure $CdIn_2Se_4$ and the nanocomposite was determined using the Scherer equation [36,56–58]. The reduction in size was found to be associated with lattice strain and a red shift in peaks. Additionally, it was observed that pure $CdIn_2Se_4$ exhibited higher crystallinity compared to the nanocomposite due to the addition of chitosan biopolymer, which enhanced its amorphous characteristics and consequently reduced the signal-to-noise ratio.

The compound $CdIn_2Se_4$ has a structure of $A^{2+}B_2^{3+}X_4^{-2}$, with cations in tetrahedral and octahedral positions, and anions arranged in a cubic closed-packed (CCP) lattice. The CCP structure consists primarily of four octahedral and eight tetrahedral sites. A ions occupy 1/8 of the tetrahedral voids, while B ions occupy 1/2 of the octahedral voids [37,59–61]. In this arrangement, Cd ions are situated in the tetrahedral sites, while in ions are situated in the octahedral sites. When encapsulated by chitosan, lattice strain occurs, causing doping of Cd ions in octahedral or unoccupied tetrahedral sites, leading to interstitial incorporation. The decrease in lattice parameters indicates the creation of $CdIn_2Se_4$@Chitosan.

The oxidation state and chemical composition of synthesized $CdIn_2Se_4$@chitosan were examined employing the XPS. As exhibited in Fig. 3a, the spectrum demonstrated the existence of Cd, In, Se, N, O and O elements. All atomic concentrations have been determined from the lowest base peaks and the findings are outlined in Table 1. Two binding energy related to $3d_{5/2}$ and $3d_{3/2}$ of Cd^{2+} centered at 405.23 eV and 412.13 eV in selenide environments are shown in Fig. 3b [38]. For In 3d (Fig. 3c), two binding energy located at 444.23 and 452.05 eV assign to $3d_{5/2}$ and $3d_{3/2}$ respectively [39]. It was also observed that the peaks of Cd and in 3d showed a redshift, indicating a decrease in energy compared to normal values [39]. This finding may be linked to the influence of chitosan, which has a lower band gap than $CdIn_2Se_4$, resulting in increased electron density around it and reduced binding energy. Fig. 3d shows the binding peak for Se 3d which are located at 54.83 and 55.90 eV and correspond to $3d_{5/2}$ and $3d_{3/2}$ [40]. This shows that Se dopant quickly forms bonds with In^{3+} and Cd^{2+} before combining with chitosan. In the C 1 s spectrum, as seen in Fig. 3e, three distinct binding peaks were observed at 284.05, 286.00, and 287.89 eV, indicating the presence of various types of bonds within the chitosan matrix such as C—C, C—H, C—N, C-O-C, C-OH, C═O, and O-C═O [41]. In Fig. 3f, two binding energies at 531.82 and 533.02 eV, which are associated with C═O, O-C═O, C—O, and O—H bonds. Additionally, the binding peaks of O 1 s were above 530 eV, indicating the production of a nanohybrid [41]. In Fig. 3 g, you can see the XPS spectrum of N 1 s, showing three peaks at 398.95, 400.03, and 401.05 eV, indicating the presence of sp^3 C—N, NH2, and O=CH-NH bonds in chitosan [42]. There was a slight change in the binding energy of N 1 s, O 1 s, and C 1 s, suggesting that the accumulation of $CdIn_2Se_4$ on the surface of chitosan may be due to chemical reactions.

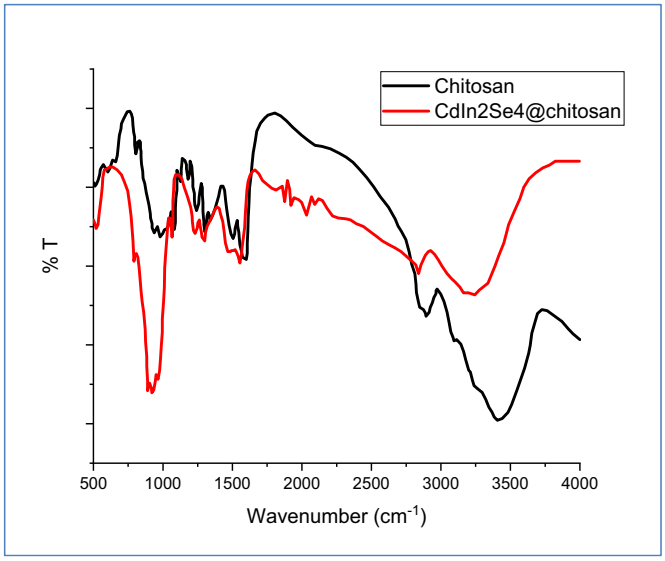

Fig. 4. FTIR spectrum of chitosan and $CdIn_2Se_4$@chitosan.

For more structural investigation, FTIR technique was used to check the functional groups in chitosan and $CdIn_2Se_4$@Chitosan surface and the results are shown in Fig. 4. The chitosan sample (Black spectrum) exhibits a shoulder peak at 1150 cm^{-1}, which corresponds to the asymmetric stretching of C-O-C bonds. Two peaks located at 1026 and 1060 cm^{-1} back to C—O stretching mode, while a small band at 895 cm^{-1} assign to the bending mode of C—H bonds in the rings of monosaccharide. $CdIn_2Se_4$@Chitosan (**Red spectrum**) displays similar spectrum to chitosan with a strong peak with range 3000–3650 cm^{-1}, which assign to the overlapping N—H and O—H bands [43,62–34].

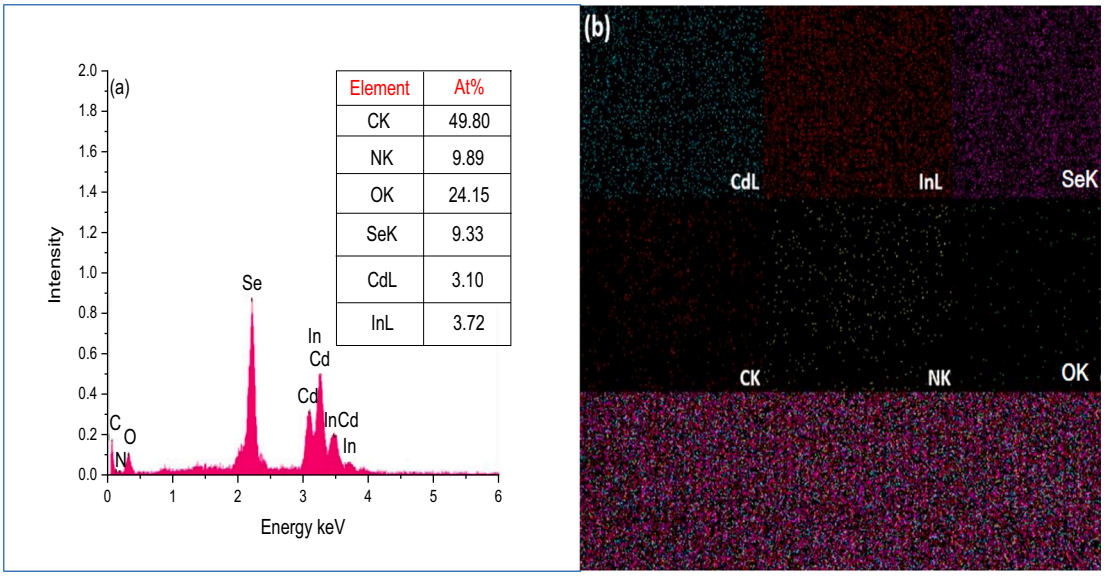

Fig. 5. (a,b) EDX-Mapping of $CdIn_2Se_4$@Ch nanocomposite.

Furthermore, there are two distinct bands at 2871 and 2952 cm^{-1} corresponding to the symmetric and asymmetric modes of C—H, which are characteristic of polysaccharides. Additionally, the spectrum reveals two bands at 1320 and 1650 cm^{-1} attributed to the stretching modes of C═O and C—N, respectively, confirming the presence of an acetyl group. A distinctive band at 1552 cm^{-1} is indicative of N—H bending mode in amide groups, along with two additional bands at 1376 and 1425 cm^{-1} corresponding to the symmetrical and bending modes of CH_3 and CH_2 [43,65–67].

The elements ratio in the CdIn2Se4@Ch nanocomposite surface were characterized by EDX-Mapping and the results are shown in Fig. 5(a,b). In Fig. 5a, the results appeared that the atomic ratio are 49.8, 9.89, 24.25, 9.33, 3.10 and 3.72, which assign to C, N, O, Se, Cd respectively, without any impurities. On the other hand, the percentage ratio of Se, Cd and In proposed that the ratio are closed to 1:2:4, as well as, the existence of C, N and O atoms are attributed to incorporating of chitosan in the prepared photocatalyst.

3.2. Morphology analysis

The prepared materials underwent morphology analysis through the use of TEM, HR-TEM, and FE-SEM in order to assess their morphology and size. The findings revealed irregularly shaped particles with distinct grain boundaries, as illustrated in Fig. 6. Fig. 6b depicted the nanometer-scale interplanar spacing, which was in agreement with the diffraction peak (222) and correlated with the X-ray diffraction (XRD) data.

The polycrystalline feature of prepared $CdIn_2Se_4$@Chitosan nanocomposite was illustrated via SAED pattern and the results are shown in Fig. 6c. Although the obtained results showed high peak intensity in XRD, they did not entirely align with the d-spacing values. This discrepancy can be attributed to the red shift observed in the XRD spectra, which indicates a relationship between 2θ and d-spacing values as per the Bragg's law. Specifically, an increase in 2θ leads to a decrease in d-spacing. Additionally, certain rings observed in the image of SAED were widely distributed, suggesting the relatively small crystal size. The presence of shining concentric rings was attributed to the high crystallinity of the $CdIn_2e_4$ photocatalyst [44,68–72]. The SAED pattern aligns with the miller index planed d-spacing obtained from the examination of XRD data. Fig. 6d illustrates a histogram with a quantitative analysis plotted using the Lorentzian function, indicating an average grain size of approximately 5 nm. The topography of the prepared $CdIn_2Se_4$@Chitosan, which includes mesoporous and microporous structures, was investigated using FE-SEM, revealing a sheet-like morphology as depicted in Fig. 6e. This suggests that the chitosan encapsulated $CdIn_2Se_4$ following agglomeration on its surface. Additionally, the results presented in Fig. 6f indicated that the prepared photocatalyst exhibited irregular morphology, with the surface of $CdIn_2Se_4$ being relatively rough and featuring some surface fractures attributed to nanocomposite formation. It is hypothesized that $CdIn_2Se_4$ and chitosan contributed to the roughness of the surface [45,73–76]. The disparate and porous shape increased pollutant adsorption, boosting the activity of photocatalytic.

3.3. Thermal analysis

The thermal analysis of prepared compounds was investigated by using DSC/TGA and the results are shown in Fig. 6. The change in sample weight was calculated using data, and the DSC was used to ascertain whether the reaction was endothermic or exothermic. The rate at which weight changes in relation to temperature was provided by the derivative of weight [46,77–80]. The TGA curve shows that the synthesized $CdIn_2Se_4$@Chitosan nanocomposite succumb three stages of degradation. A weight loss of 9.12 % was observed initially, attributed to water evaporation. Subsequently, at 220 °C, a second degradation stage resulted in a slightly higher mass loss of 19.34 %, ascribed to the disruption of physical interactions between the inorganic and organic components. The third stage, occurring at 340 °C, involved the degradation of chitosan, leading to a weight loss of approximately 6.54 %. The prepared $CdIn_2Se_4$@Chitosan nanocomposite exhibited consistent weight stability at temperatures up to 700 °C, with a heating rate of 15 °C/min. However, at 70–80 °C, the sample experienced weight loss due to water evaporation. The evaporation of water ligands and adsorbed water resulted in an endothermic peak at approximately 70–80 °C. Conversely, no endothermic transition was observed when the temperature was raised from 25 to 30 °C, indicating no phase alteration in the synthesized $CdIn_2Se_4$@Chitosan nanocomposite [47,81–94]. At a temperature of 320 °C, the results indicate a pronounced exothermic peak attributed to the oxidative degradation of the sample due to the structural stability of the self-assembling $CdIn_2Se_4$@Chitosan, which was largely influenced by the chelation process involving the amine chitosan group. Additionally, the TGA curve correlated with the DSC, thus confirming the sudden change in weight during both endothermic and exothermic degradation of the nanocomposite at 75 °C and 320 °C.

The absorbance spectra of pure $CdIn_2Se_4$ and $CdIn_2Se_4$@Chitosan

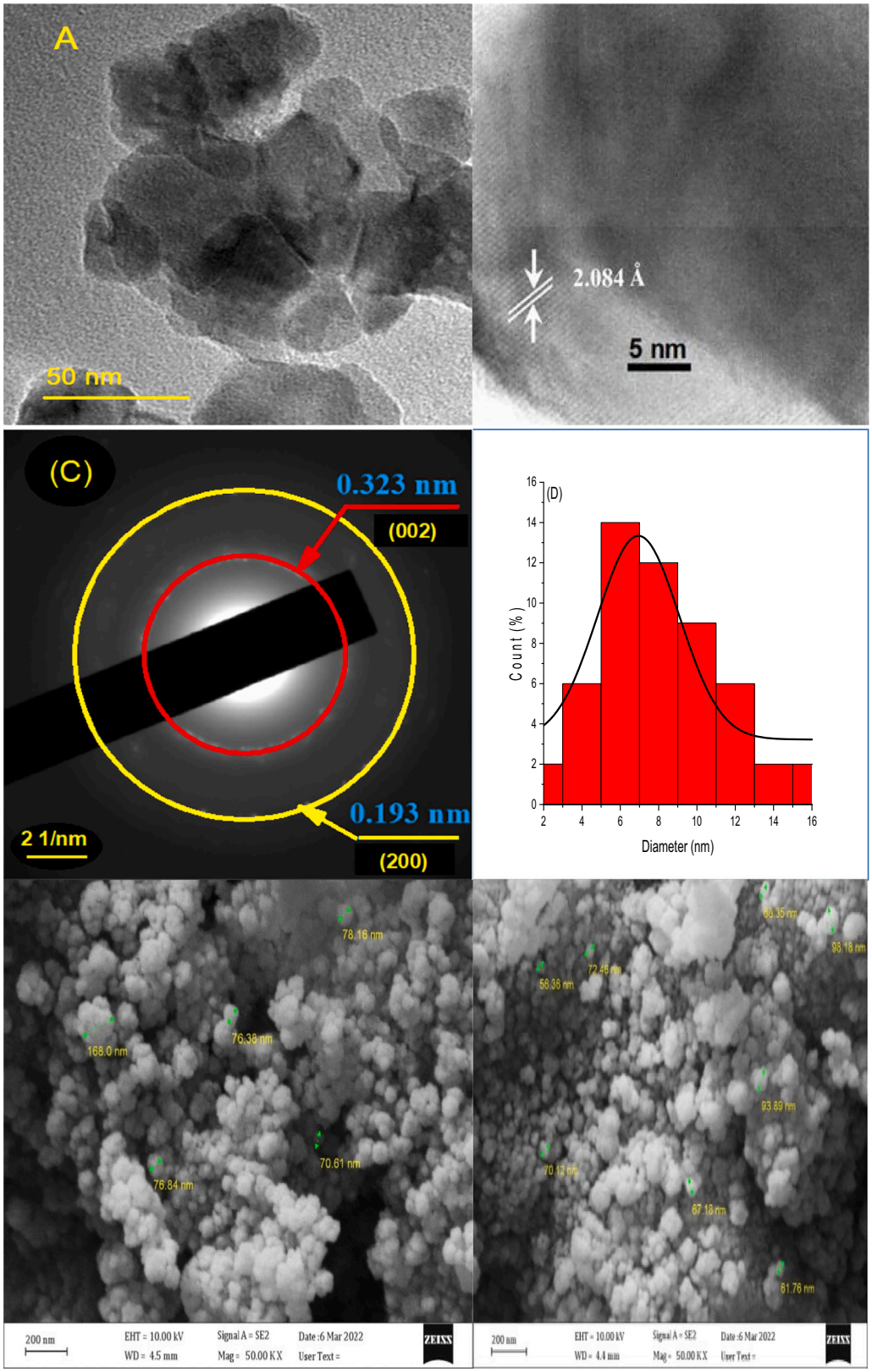

Fig. 6. (a,e) TEM and FESEM analysis of CdIn2Se4@Ch, (b) HR-TEM image, (c) SAED pattern, (d) histogram particles distribution carve, (f) FESEM of CdIn2Se4.

were analyzed in the 200-800 nm range using Diffuse Reflectance Spectroscopy (DRS) to gain insight into their spectral characteristics. The results, depicted in Fig. 7a, revealed that pure $CdIn_2Se_4$ exhibited a broad band with an edge at approximately 600 nm. In contrast, the composite sample showed a shift in the edge towards longer wavelengths, indicating the formation of a heterojunction composite. This shift in edge absorption suggested the transfer of electrons from the valence band (VB) to the conduction band (CB), thereby inhibiting the recombination process. Furthermore, Tauc curve analysis was utilized to determine the indirect bandgap of the synthesized compounds. The

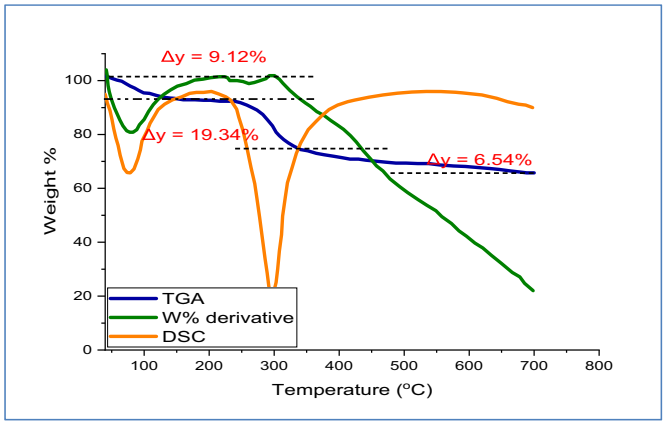

Fig. 7. TGA/DSC analysis $CdIn_2Se_4$@Chitosan.

findings in Fig. 7b indicate that the bandgap of the chitosan-incorporated sample increased compared to the pristine sample, suggesting a smaller particle size. To further investigate, PL spectroscopy was used to analyze the spectrum characteristics of the synthesized photocatalysts. PL is a reliable method for assessing the recombination process of electron-hole pairs in the synthesized compounds. In Fig. 7c, the emission spectra resulting from exciting the compounds at 330 nm were examined. The results showed that the spectra of $CdIn_2Se_4$@Chitosan are similar to those of the pristine compound but with lower intensity. The study showed that a lower PL intensity can lead to better separation of charges and a slower recombination process [48,85–89]. Additionally, the results revealed a distinct peak at 373 nm, which is associated with the excitation of electrons from VB to CB in the original sample [49,90–92]. These findings suggest that the synthesized $CdIn_2Se_4$ may have greater charge separation and photocatalytic activity compared to the original sample.

4. Photocatalytic performance

4.1. Impact of H_2O_2 dosage

H_2O_2 plays a significant role in the oxidation process. When H_2O_2 is irradiated, it produces OH* and interacts with the photocatalyst to form them. Therefore, it's important to study and understand its impact on the photodegradation of ofloxacin and 2,4-dichlorophenoxyacetic using synthesized pristine and $CdIn_2Se_4$@Chitosan. For this purpose, H_2O_2 was varied within the range of 0.3–1.5 μL/ml in a solution containing (50 mL, 15 ppm) of ofloxacin and (50 mL, 10 ppm) of 2,4-dichlorophenoxyacetic. The findings (Fig. 9a,c) showed that the photocatalytic activity increased up to 0.6 μL/mL and 0.9 μL/mL for ofloxacin and 2,4-dichlorophenoxyacetic, respectively. However, there was a noticeable decrease after increasing the H_2O_2 dosage. The initial increase may be attributed to the decomposition of H_2O_2 due to sunlight exposure, leading to the formation of hydroxyl free radicals (Eq.5). On the other hand, the decrease in efficiency with higher H_2O_2 dosage could be due to the self-scavenging of OH free radicals by excess peroxide (Eq.6) [50,93–96].

$$H_2O_2 \xrightarrow{hv} 2OH^* \quad (5)$$

$$H_2O_2 + OH^* \rightarrow H_2O + O_2H^* \quad (6)$$

Additionally, the synthesized photocatalyst also contributes to the generation of hydroxyl free radicals in sunlight [51], which leads to the production of e–h + pairs that interact with OH ions and H_2O_2 to produce hydroxyl free radicals as shown in Eq. (7–10). The findings indicate that the photodegradation efficiency reached 82 % and 92 % for ofloxacin and 2,4-dichlorophenoxyacetic acid, respectively, when using 0.6 and 0.9 μl/ml of H_2O_2 dosage with reaction rates of 0.017 and 0.023 min-1 (Fig. 9b,d).

$$CdIn2Se4@Chitosan \xrightarrow{hv} e^- + h^+ \quad (7)$$

$$H_2O + e^- \rightarrow OH^* + OH^- \quad (8)$$

$$H_2O \rightarrow OH^- + OH^* \quad (9)$$

$$OH^- + h^+ \rightarrow OH^* \quad (10)$$

4.2. pH impact

The pH of the solution is mainly determined by the surface charge of the prepared $CdIn_2Se_4$@chirosan nanocomposite. It is important to find the best pH for degrading pollutants in wastewater, taking into account the types of contaminants present [52,97–101]. The pH at which the solution has a zero-point charge was determined by adjusting the pH from 2 to 12 using 1 M HCl and NaOH through the DLS technique. The investigation revealed that when using 0.01 g of $CdIn_2Se_4$@Chitosan, the ZPC is 6.5. The pH level plays a crucial role in the effectiveness of the catalytic photodegradation process, and it also affects the efficiency of the synthesized catalyst. The pH of the solution is set before exposing it to sunlight, and it remains unchanged during the reaction. The study utilized a pH range of 2–12 to observe how it impacts the photodegradation of ofloxacin and 2,4-dichlorophenoxyacetic. The initial concentration of ofloxacin was 15 ppm, and the $CdIn_2Se_4$@Chitosan dose was maintained at 0.08 g with 0.6 ml of hydrogen peroxide. The results indicated that the optimal pH for high degradation efficiency was 7, achieving an 82 % degradation rate with a constant rate of 0.017 min^{-1}. An improvement in efficiency was seen up to pH 7, but a decrease in performance was noticed after that (Fig. 10a). This is because there is a nitrogen atom present in position 4 of the piperazinyl group, making it anionic above $pKa_2 = 8.11$, cationic below $pKa_1 = 6.05$, and neutral (zwitterion) between pKa_1 and pKa_2 [53,102–105]. The pH effect on ofloxacin is not shown in terms of ionization state for $CdIn_2Se_4$@chitosan and ofloxacin, as both can carry positive or negative charges in acidic or alkaline conditions [54]. When the pH is high, the OH free radicals are considered as the initial oxidation species, while at low levels of pH, the positive holes are considered as the initial species [55]. Based on the findings and the excess of hydroxyl free radicals due to H_2O_2, it can be concluded that the oxidative transition of ofloxacin is primarily caused by free radicals rather than holes. The impact of pH on the photodegradation of 2,4-dichlorophenoxyacetic was investigated using 10 ppm of pollutant in a 50 ml solution with 0.08 mg of $CdIn_2Se_4$@Chitosan and 0.9 ml of H_2O_2.The findings show that the catalyst's ability to break down under light decreases as the pH level rises from 2 to 12 (Fig. 10c). The best pH level is 3, where it achieves a maximum efficiency of 94 % and a rate constant of 0.033 min^{-1}. The decrease in efficiency as the pH increases might be due to the presence of hydroxyl ions, which hinder radical formation by either overlapping or reacting with it. Moreover, at low pH levels, peroxide breaks down to form hydroxyl radicals, while the recombination rate of radicals decreases [56,106–110].

4.3. Catalyst dosage impact

The H_2O_2 dosage, reaction premier pollutant concentration and pH were fixed at 0.6 and 0.9 ml, 15 and 10 ppm and 7 and 3, respectively, to investigate the $CdIn_2Se_4$@chitosan impacts on the ofloxacin and 2,4-dichlorophenoxyacetic photodegradation. The amount of $CdIn_2Se_4$@-chitosan used ranged from 0.03 to 0.16 g in a 50 ml solution [107–110]. The results displayed in Fig. 11a,c indicated that the photodegradation activity increased as the catalyst dosage was raised, reaching its peak at 0.1 and 0.13 mg for ofloxacin and 2,4-dichlorophenoxyacetic, before slightly decreasing. A higher efficiency in photocatalysis can be

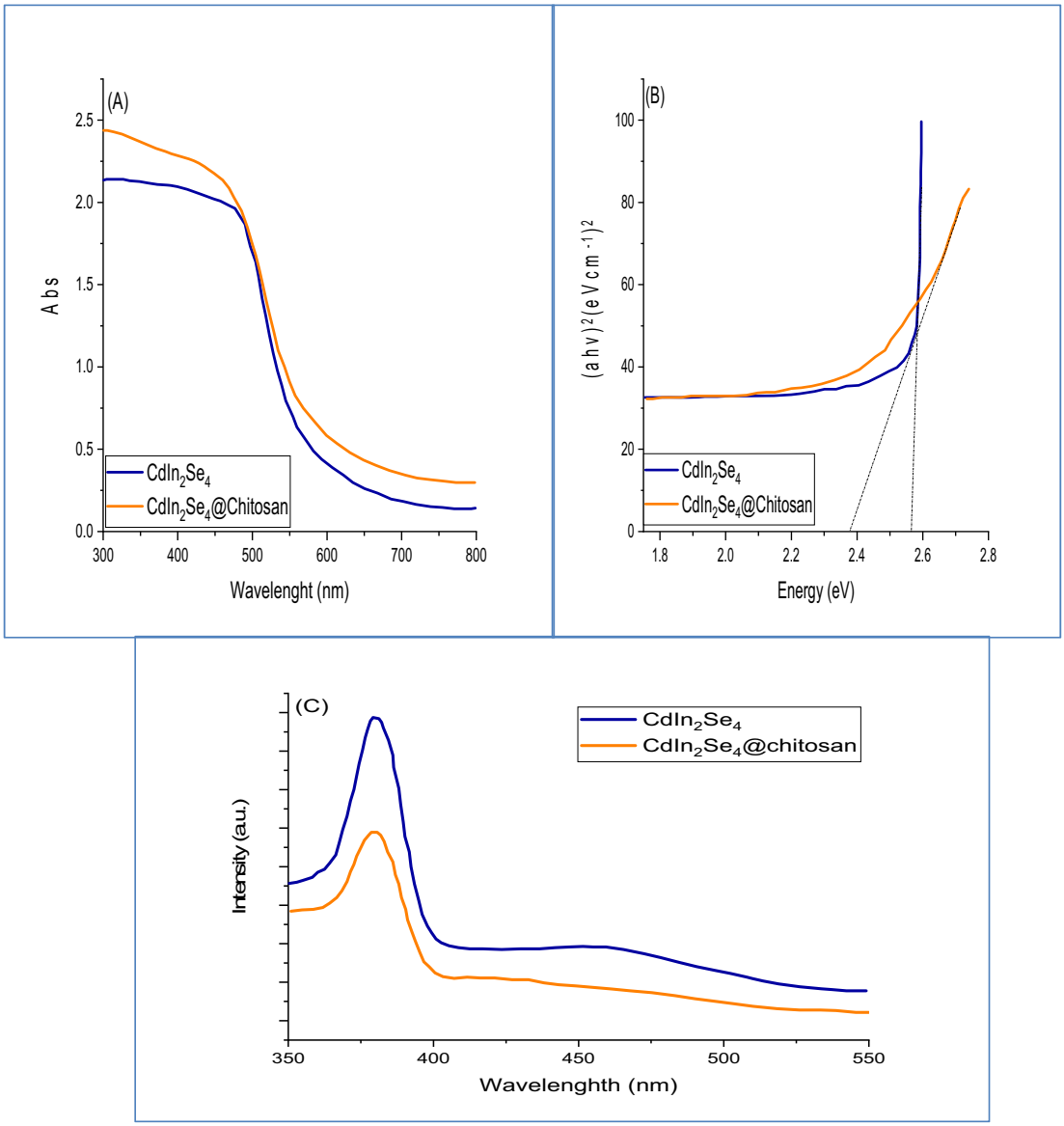

Fig. 8. (a,b) UV–Vis spectrum and Tauc plot of CdIn2Se4 and CdIn2Se4@Chitosan nanocomposite, (c) PL spectrum of synthesized of CdIn2Se4 and CdIn2Se4@-Chitosan nanocomposite.

attributed to an increase in active sites generated by the addition of more photocatalyst. However, adding more photocatalyst resulted in reduced effectiveness of photocatalysis due to the increased opacity of the solution, leading to scattered light which hindered the introduction of photons into the suspension [57,111–113]. Also, due to the presence of H_2O_2, increasing the amount of photocatalyst resulted in an increase in the production of OH free radicals. However, an excess of OH free radicals may lead to a recombination process at high doses [58,114–118]. Therefore, it can be inferred that the enhancement of $CdIn_2Se_4$@chitosan is significant as it reduces the excessive use of the catalyst. As shown in results, the increased dosage led to a maximum efficiency of 88 and 96 % for ofloxacin and 2,4-dichlorop.

4.4. Pollutants concentration impact

To study how ofloxacin and 2,4-dichlorophenoxyacetic acid affect the environment, we set the best conditions: pH at 7, catalyst dosage at 0.1 and 0.13, H_2O_2 volume at 0.3 and 0.6 ml, and pollutant concentration from 5 to 30 ppm. Ofloxacin and 2,4-dichlorophenoxyacetic acid are found in water at concentrations ranging from μg/L to mg/L. Even though these high initial concentrations are commonly used in studies on the photodegradation process to determine concentration changes and identify transformation products, they can be delicate to estimate [119–121]. Following an initial increase in ofloxacin and 2,4-dichlorophenoxyacetic acid concentrations, a slight improvement was observed up to 20 and 15 ppm (ppm), after which a slight decrease occurred (Fig. 12a,c). The narrow paths for the movement of light through the photos may be mainly responsible for the slight decrease in the breakdown of ofloxacin and 2,4-dichlorophenoxyacetic acid when their concentrations are increased [59,122–123]. Additionally, higher concentrations of pollutants would need an additional catalyst, make the solution more opaque, and hinder the breakdown process through exposure to light [60,124–126]. Also, As the levels of ofloxacin and 2,4-dichlorophenoxyacetic acid rose, the pollutants began to take up more active sites, gradually pushing out the O_2 and OH ions that had been adsorbed on the surface. This caused the catalyst to produce fewer OH free radicals and superoxide anion radicals over time, leading to decreased efficiency. All reaction parameters improved, resulting in a higher degradation efficacy of ofloxacin and 2,4-dichlorophenoxyacetic acid through $CdIn_2Se_4$@chitosan, reaching 85 % and 96 % respectively

Table 2
Quantum yield and FoM for removing of ofloxacin and 2,4-dichlorophenoxyacetic at different system.

Cata.	Quantum efficiency (molecules/photon)		Figure of Merit (FoM)	
	Ofloxacin	2,4-dichlorophenoxyacetic	Ofloxacin	2,4-Dichlorophenoxyacetic
Photolysis	$5*10^{-7}$	$3.3*10^{-3}$	$1.2*10^{-6}$	$4.8*10^{-6}$
Photolysis+H_2O_2	$7.3*10^{-7}$	$4.2*10^{-6}$	$1.8*10^{-6}$	$5.9*10^{-6}$
$CdIn_2Se_4$	$4.3*10^{-5}$	$1.6*10^{-4}$	$1*10^{-4}$	$2.4*10^{-4}$
$CdIn_2Se_4$+ H_2O_2	$6.5*10^{-5}$	$2.5*10^{-4}$	$1.6*10^{-4}$	$3.7*10^{-4}$
$CdIn_2Se_4$@Ch	$6.7*10^{-5}$	$2.1*10^{-4}$	$1.6*10^{-4}$	$3.1*10^{-4}$
$CdIn_2Se_4$@Ch + H_2O_2	$8.1*10^{-5}$	$5.3*10^{-4}$	$2*10^{-4}$	$7.7*10^{-4}$

with rate constants of 0.0251 and 0.047 min^{-1} (Fig. 12b,d).

4.5. Exposure time impact

The irradiation time impact was investigated in optima conditions for ofloxacin and 2,4-dichlorophenoxyacetic at $CdIn_2Se_4$@chitosan dosages of 0.1 and 0.13 g and a pollutant concentration of 5 and 10 ppm. In Fig. 13a,b, all different groups were studied to understand how the photocatalytic activity changes over time. It was found that there was no further decrease in the concentration of ofloxacin and 2,4-dichlorophenoxyacetic after 90 min. These results may be due to the exhaustion of $CdIn_2Se_4$@chitosan active sites. The findings indicate that using

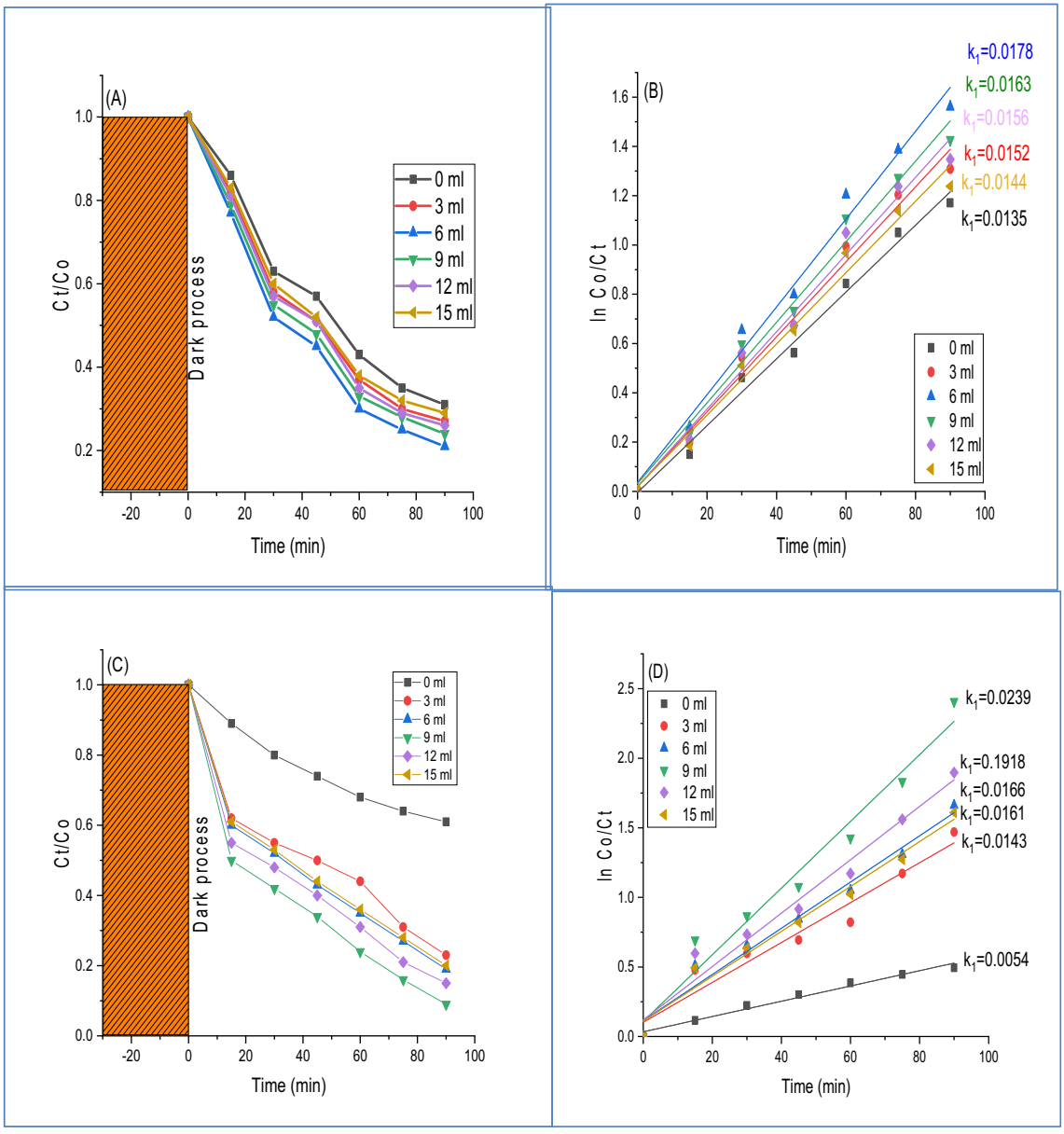

Fig. 9. H_2O_2 dosage impact on the photodegradation of (a) ofloxacin, (c) 2,4 dichlorophenoxyacetic; degradation kinetics for (b) ofloxacin and (d) 2,4 dichlorophenoxyacetic.

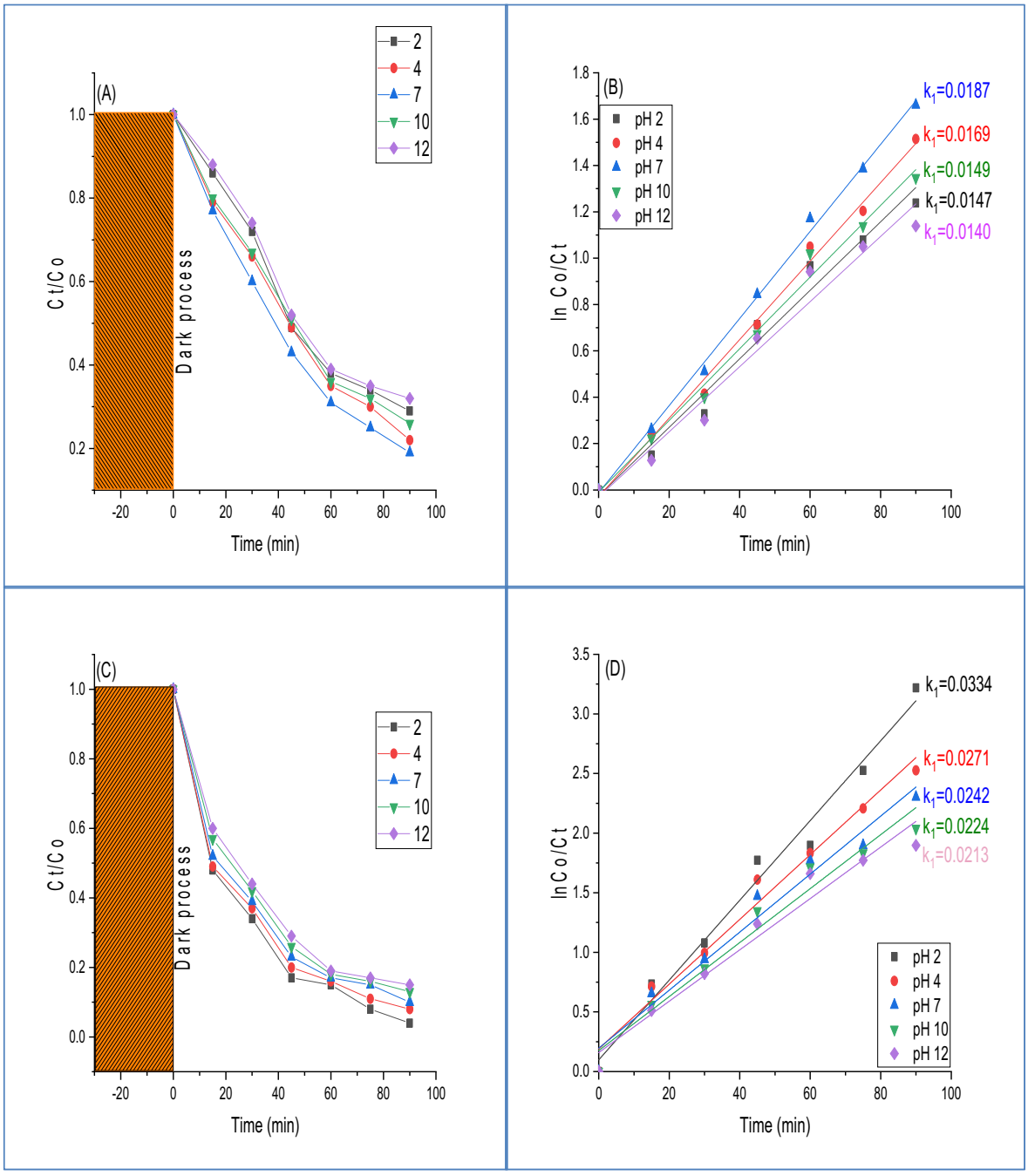

Fig. 10. pH impact on the photodegradation of (a) ofloxacin, (c) 2,4 dichlorophenoxyacetic; degradation kinetics for (b) ofloxacin and (d) 2,4 dichlorophenoxyacetic.

$CdIn_2Se_4$@chitosan nanocomposite with hydrogen peroxide led to maximum degradation of 85 % for ofloxacin and 96 % for 2,4-dichlorophenoxyacetic. No changes in pollutant concentration were observed during photolysis, indicating that photodegradation only occurred in the presence of $CdIn_2Se_4$@chitosan or H_2O_2. In Fig. 13c, we can see how different systems compare in terms of degradation efficiency. It was observed that $CdIn_2Se_4$@chitosan, when combined with hydrogen peroxide, achieved degradation efficiencies of 86 % for ofloxacin and 95 % for 2,4-dichlorophenoxyacetic. Additionally, as shown in Fig. 13d and e, the total COD decreased by 80.6 % and 88.3 % from their original concentration values for ofloxacin and 2,4-dichlorophenoxyacetic. During the photodegradation of these compounds, intermediate products are formed which can be identified through LCMS analysis. The chemicals in the middle of the process may have helped to protect against the large amount of harmful substances produced by the photocatalyst, which could have limited how much COD decreased. The catalyst that was created was also used to break down other chemicals like congo red, methylene orange, rhodamine B, and sulfomethaxozole. The pollutants' levels were 20 ppm and they broke down at pH 7 using 10 mg of photocatalyst. There was a slight decrease in the efficiency of breaking down 2,4-dichlorophenoxyacetic when the pH was higher than optimal. Even though the created photocatalyst worked well for breaking down dyes, this project focused on getting rid of harmful pollutants (ofloxacin and 2,4-dichlorophenoxyacetic) after a period where there wasn't much research done (see Fig. 13f). It's also safe to say that the catalyst that was prepared is effective at getting rid of almost

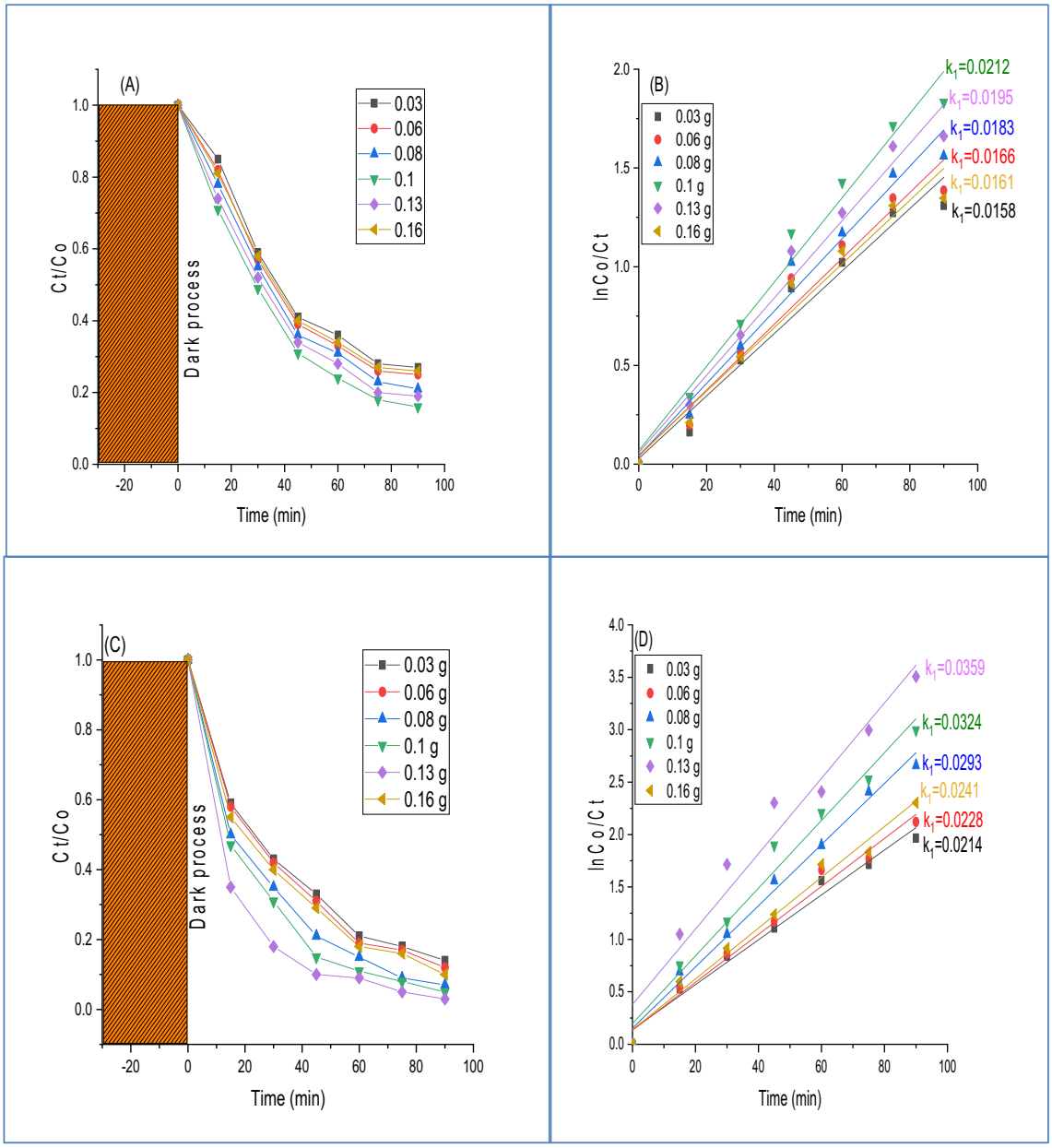

Fig. 11. catalyst dosage impact on the photodegradation of (a) ofloxacin, (c) 2,4 dichlorophenoxyacetic; degradation kinetics for (b) ofloxacin and (d) 2,4 dichlorophenoxyacetic.

all pollutants and can be used in water treatment.

4.6. *Effect of temperature*

The study looked at how different temperatures affect the efficiency of photodegradation, focusing on a temperature range of 10 to 40 degrees Celsius. The results in Fig. 14a,c indicate that the performance of the synthesized $CdIn_2Se_4$@ch photocatalyst decreases slightly as the temperature increases for ofloxacin and 2,4-dichlorophenoxyacetic. While higher temperatures lead to more collisions and improved performance over time, this only contributes a small amount to the overall increase in reaction rate [61,127–130]. The depressed adsorption of the ofloxacin and 2,4-dichlorophenoxy on the CdIn2Se4@Chitosan is attributed to the high energy of kinetic, which obscures the advantage effect of higher collision recurrence. This causes the recombination of the ROS that have been generated, leading to a decrease in the efficiency of degradation [62]. The Fig. 14b,d show the reduction in rate of photodegradation.

Additionally, there was a significant decrease in the degradation efficiency in other composites such as pure $CdIn_2Se_4$ with and without hydrogen peroxide, and $CdIn_2Se_4$@Chitosan as depicted in Fig. 15. The study of photodegradation of ofloxacin and 2,4-dichlorophenoxyacetic revealed that the relatively fast recombination of electrons and holes contributed to the reduction in efficiencies, which can be highlighted by PL spectroscopy (Fig. 8c). One effective way to improve the performance of the synthesized $CdIn_2Se_4$@Chitosan nanocomposite is by adding H_2O_2, which can help reduce the recombination of e–h + pairs by accepting electrons [63]. Additionally, researchers looked into the removal efficiency of TOC for ofloxacin and 2,4-dichlorophenoxyacetic in different systems. The $CdIn_2Se_4$@chitosan nanocomposite showed the highest mineralization with hydrogen peroxide, reaching 73 % and 86 % activity for ofloxacin and 2,4-dichlorophenoxyacetic under optimal conditions. The effectiveness of mineralization was confirmed through LCMS analysis, revealing the breakdown of large pollutant molecules

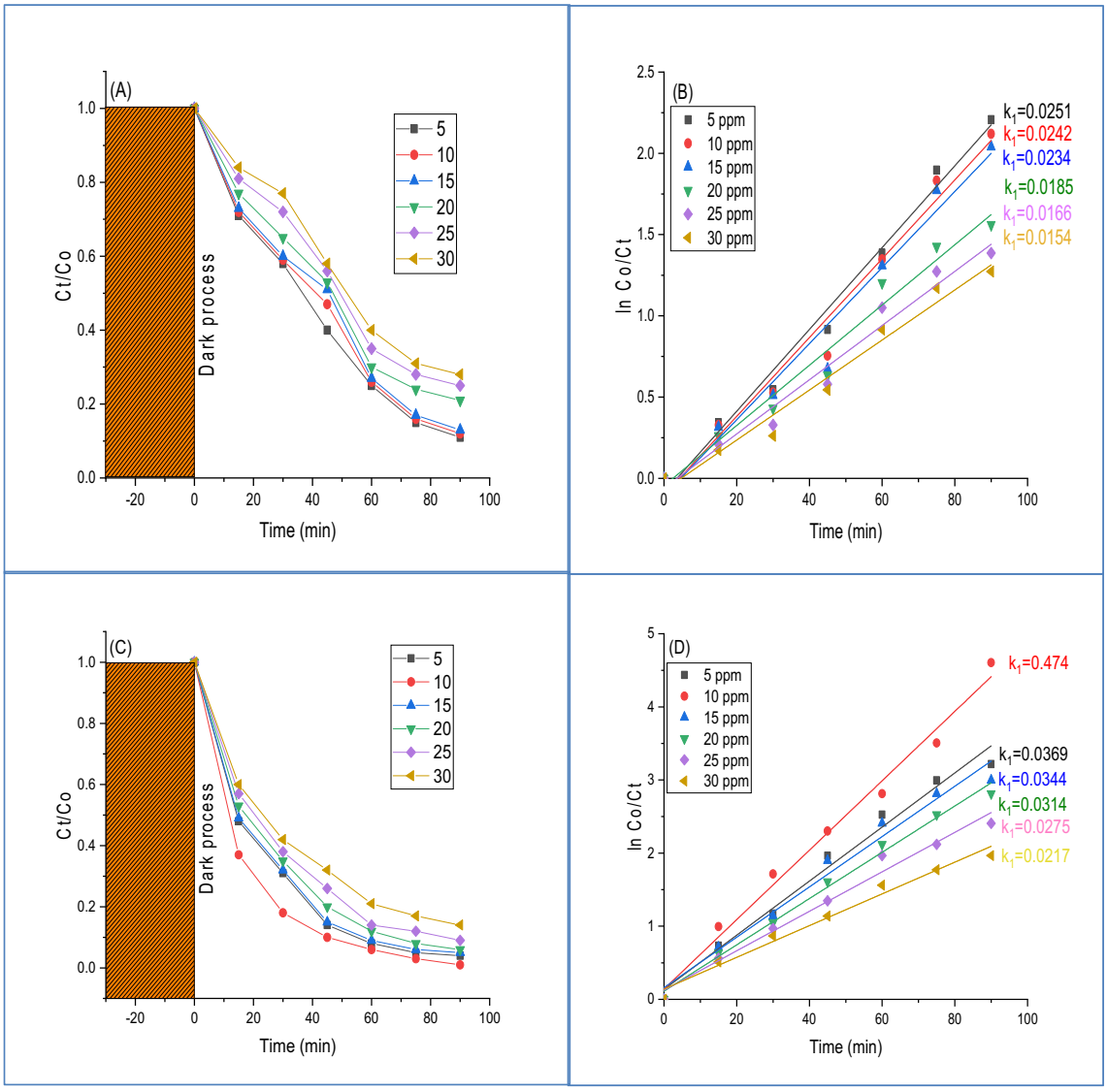

Fig. 12. Catalyst dosage impact on the photodegradation of (a) ofloxacin, (c) 2,4 dichlorophenoxyacetic; degradation kinetics for (b) ofloxacin and (d) 2,4 dichlorophenoxyacetic.

into smaller ones. Additionally, quantum yield and FOM calculations were used to assess the performance of $CdIn_2Se_4$@chitosan in the presence and absence of hydrogen peroxide. The study found that the nanocomposite produced the highest quantum yield and FOM of $8.12*10^{-5}$ molecules/photon and $2.06*10^{-4}$, and $5.38*10^{-4}$ molecules/photon and $7.78*10^{-4}$ for ofloxacin and 2,4-dichlorophenoxyacetic, when H_2O_2 was present, compared to lower quantum yield and FOM of 6.71*10–5 molecules/photon and $1.69*10^{-4}$, and $2.16*10^{-4}$ molecules/photon and $3.14*10^{-4}$ in the absence of H_2O_2. The degradation of ofloxacin and 2,4-dichlorophenoxyacetic in the presence of different compounds was investigated to support previous findings. When comparing the synthesized nanocomposite with previously published papers (Table 2), it was observed that our synthesized photocatalyst demonstrated effective degradation at low dosage and sunlight exposure, unlike the earlier studies where degradation occurred at higher levels or under different conditions.

4.7. Effect of scavenger

It is widely known that the electrons and holes produced by light have a direct impact on the speed of the process that breaks down certain chemicals when exposed to light [64]. To determine which of these particles plays a major role in breaking down ofloxacin and 2,4-dichlorophenoxyacetic acid during photodegradation, various scavenger agents were added during the degradation process to capture them. This study aimed to provide a thorough and accurate assessment of how ROSs are involved. Scavengers such as benzoic acid, benzoquinone, silver nitrate, and triethanolamine were used to capture hydroxyl radicals, superoxide anions, electrons, and holes respectively. The study found that using OH* and $*O_2^-$ scavengers reduced the efficiency of ofloxacin photodegradation to 25 % and 32 %, as shown in Fig. 16. For 2,4-dichlorophenoxyacetic, the reduction was to 35 % and 40 %. However, silver nitrate and triethanolamine had a minimal impact on the performance of photocatalytic for $CdIn_2Se_4$@chitosan nanocomposite in degrading ofloxacin and 2,4-dichlorophenoxyacetic. This research provides important information about the role of hydroxyl free radical and super oxide anion in the photodegradation of these compounds [65], while also indicating the limited involvement of electron-hole pairs.

4.8. Effect of co-existing species

Various cations are present in wastewater, so their impact was

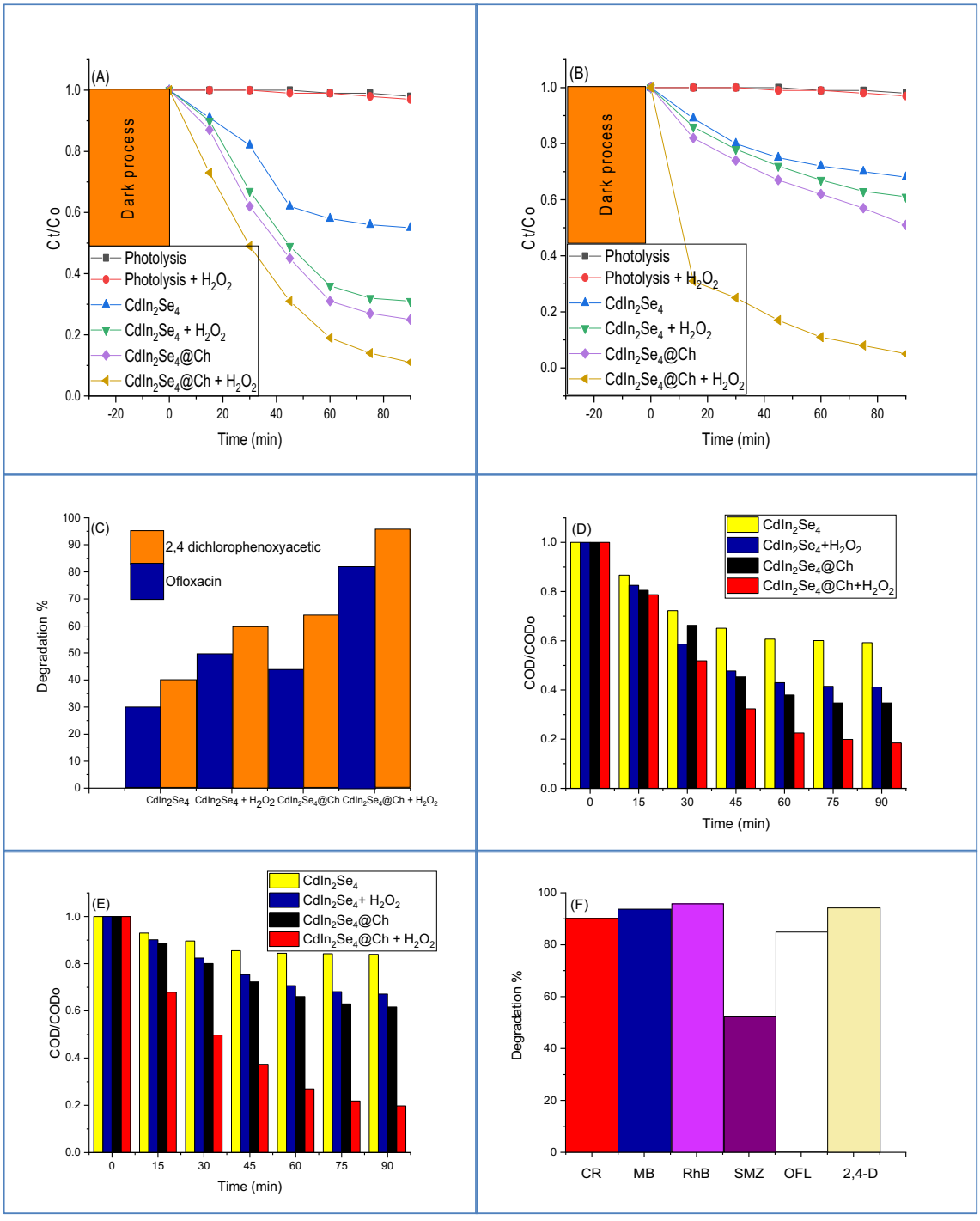

Fig. 13. Effect of contact time on degradation of (a) ofloxacin, (b) 2,4-dichlorophenoxyacetic, (c) performance of degradation by different catalyst, COD analysis on for degradation (d) ofloxacin, (e) 2,4-dichlorophenoxyacetic, performance of photodegradation on different pollutants.

examined using 0.02 M solutions of potassium, magnesium, and aluminum sulphate. These ions are stable and do not interfere with the photodegradation process [66]. Fig. 17 illustrates the photodegradation performance of the synthesized $CdIn_2Se_4$@chitosan nanocomposite in the presence of specific cations. The degradation of Ofloxacin was inhibited to varying degrees in the presence of these ions. It can be inferred that the SO_4^{2-} ions may have contributed to the inhibition due to their limited influence. Notably, aluminum salt exhibited the most significant suppression of photocatalysis (38 %), possibly attributed to Al^{3+} ions binding to the catalyst surface, thereby obstructing active sites and reducing photocatalytic efficiency. Additionally, calcium ions showed a higher repression in photodegradation capability (51 %) compared to sodium ions (55 %), likely due to their larger ionic size [67]. In this study, a 0.02 M concentration of I^-, Cl^-, and SO_4^{2-} was introduced to examine the impact of various inorganic anions on the photodegradation capacity of the synthesized $CdIn_2Se_4$@Ch nanocomposite (Fig. 17b). A decrease in efficiency was observed with the introduction of these specific anions. It was found that these anions interacted with hydroxyl free radicals, leading to the quenching of pollutant degradation and a reduction in efficiency. Additionally, upon adsorption to the surface, these anions reacted with holes to generate Cl^- and SO_4^{2-} radicals, which then interacted with electrons to regenerate the anion, as

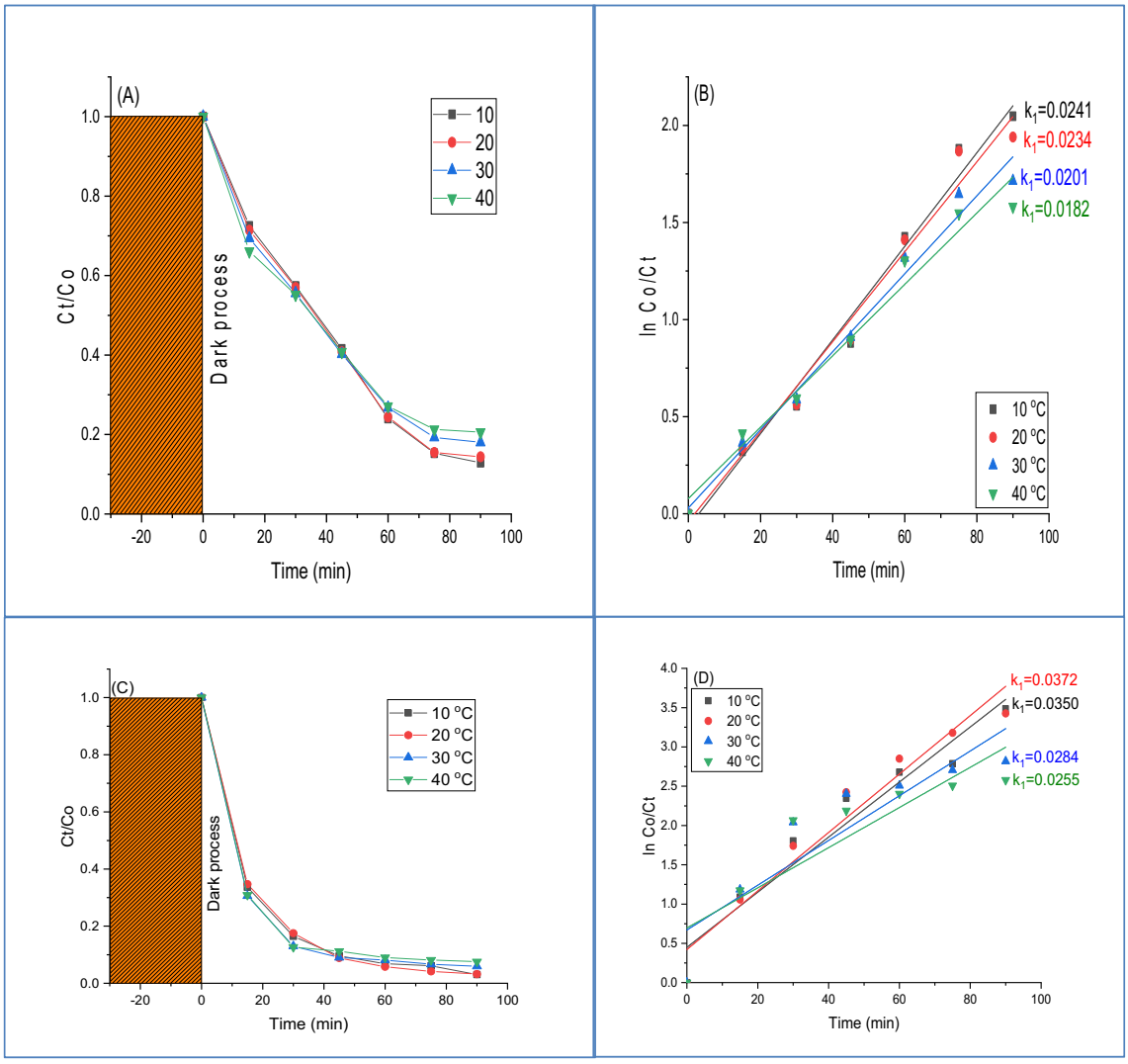

Fig. 14. Temperature effect on photodegradation (a) ofloxacin, (c) 2,4-dichlorophenoxyacetic degradation kinetics for (b) ofloxacin and (d) 2,4 dichlorophenoxyacetic.

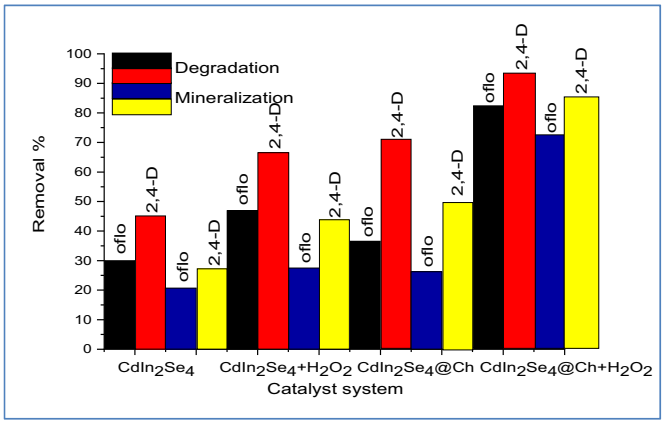

Fig. 15. Effect of catalyst system on degradation and mineralization.

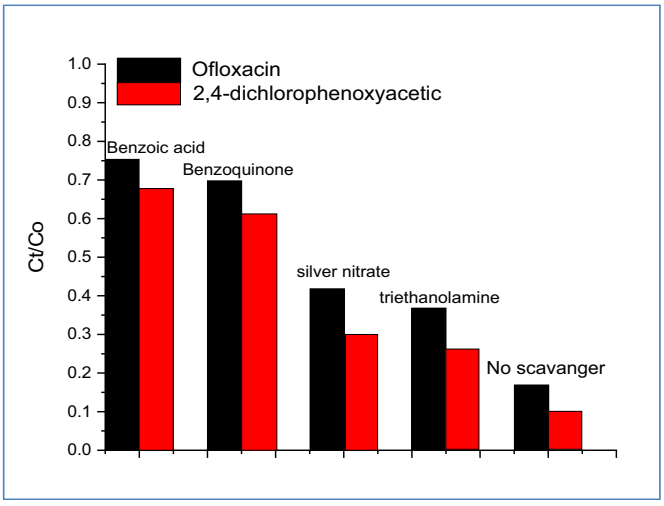

Fig. 16. Effect of scavenger on degradation of ofla and 2,4-D at optimum conditions.

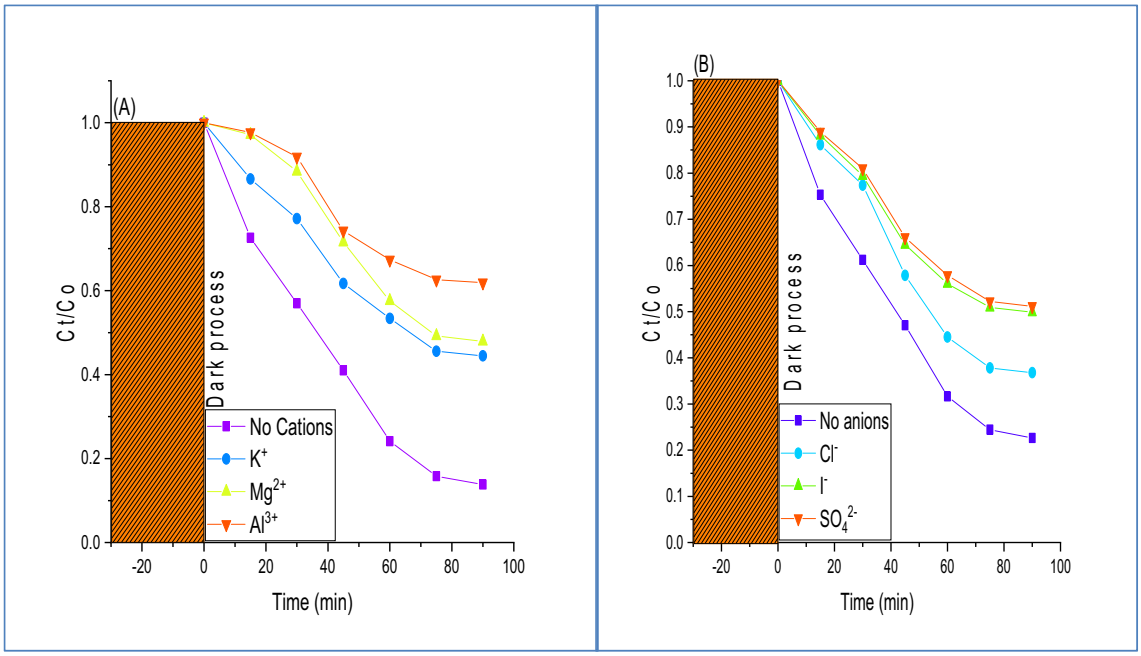

Fig. 17. effect of (a) cations and (b) anions on ofloxacin removal by $CdIn_2Se_4$@Ch.

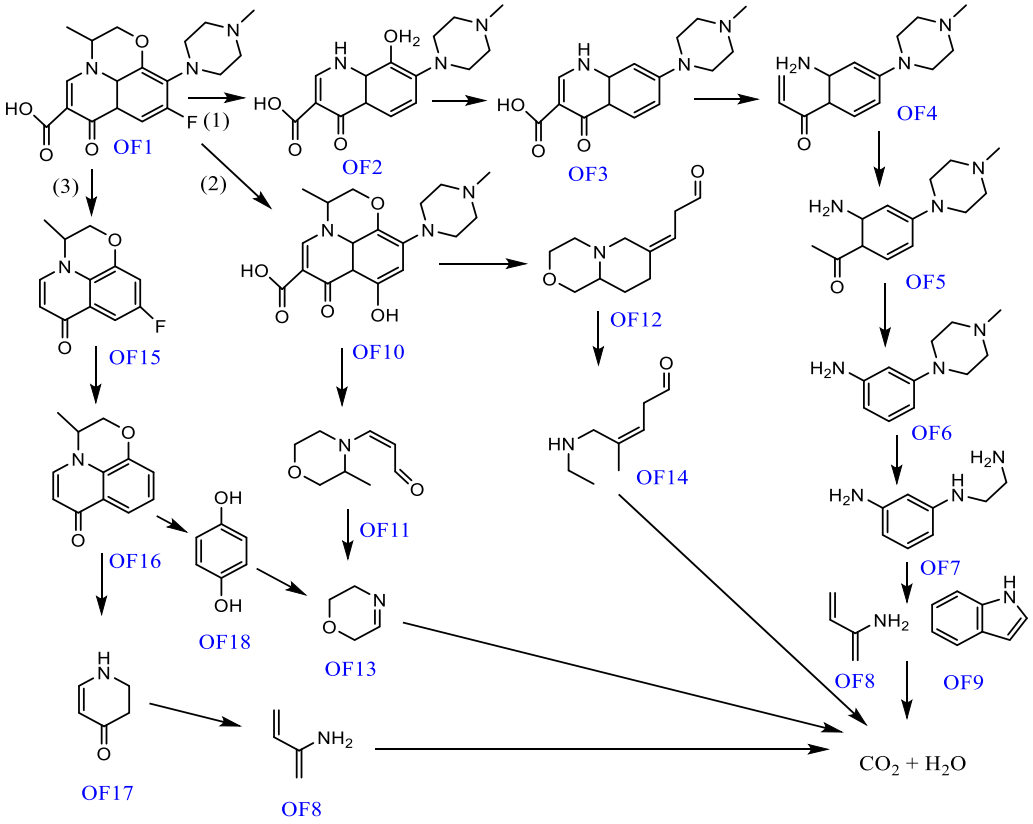

Fig. 18. Possible pathways for photodegradation of ofloxacin using $CdIn_2Se_4$@Ch.

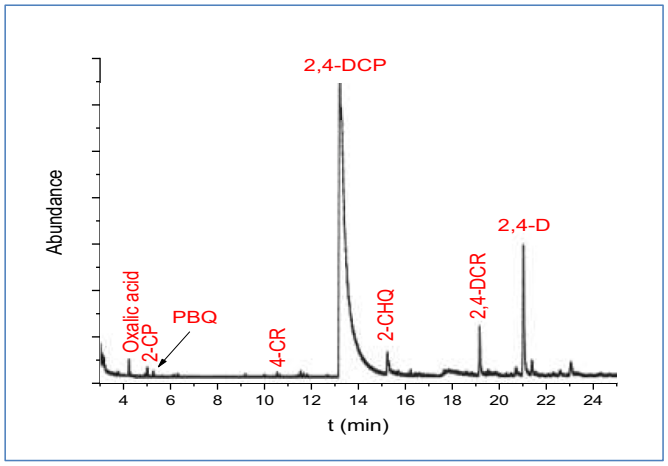

Fig. 19. LC-MS analysis of the formed intermediates during photodegradation of 2,4-D pollutant.

demonstrated in Eqs. (11)–(13).

$$I^-/SO_4^{2-} + h^+ \rightarrow {}^*I/SO_4{}^{*-} \quad (11)$$

$${}^*OH + I^-/SO_4^{2-} \rightarrow {}^*I/SO_4{}^{*-} + OH^- \quad (12)$$

$${}^*I/SO_4{}^{*-} + e^- \rightarrow I^-/SO_4^{2-} \quad (13)$$

Iodine anions exhibited greater photocatalytic activity than sulfate anions, attributed to their larger size. Conversely, F^- ions are noteworthy for their exceptional resistance to oxidation by holes [68]. They have the capacity to coat the catalyst surface, hindering the production of hydroxyl free radicals. The decrease in efficiency was observed to be directly linked to the increase in surface coverage by Cl^- ions as their concentration increased. Thus, in the presence of iodine, the initial production of hydroxyl free radicals in the solution slightly reduces efficiency.

4.9. LC-mass analysis

A LC-MS analysis was conducted to investigate potential degradation pathways and intermediates resulting from the breakdown of ofloxacin and 2,4-dichlorophenoxyacetic acid. Fig. 18 shows three reasonable pathways and eighteen intermediate products for the transformation of ofloxacin. The initial pathway involves removing fluorine and breaking the morpholine ring, then proceeding with reduction and decarboxylation to produce OF5 ($m/z = 233$). The ring splitting results in the cleavage of large molecules into smaller OF8 and OF9 ($m/z = 69$ and 118), which are further mineralized into CO_2 and H_2O·In the second pathway, removal of fluorine leads to OF10 ($m/z = 358$), followed by collapse into smaller aliphatic (OF14; $m/z = 141$) and aromatic molecules (OF13; $m/z = 85$) through two distinct pathways. The third pathway involves carboxyl group removal, followed by piperazine ring elimination, resulting in the formation of OF15 ($m/z = 218$). Subsequent removal of a fluorine atom leads to dissociation into smaller molecules, OF17 and OF18 ($m/z = 110$, 97). Furthermore, the smaller molecules obtained from different pathways underwent mineralization to produce CO_2 and H_2O. The LC-MS analysis of the photodegradation of 2,4-dichlorophenoxyacetic acid revealed several products, including 2-chlorophenol, 2-chlorohydroquinone, 2,4-dichlorophenol, 4-chloro-1,3-benzenediol, p-benzoquinone, 4,6-dichlororesorcinol, and various small-molecule acids such as oxalic and glycolic acids. The previous research also identified a range of intermediate compounds that could be linked to different oxidation processes utilized in these experiments. Based on the compounds identified during the CdIn2Se4@Chitosan oxidation process, it was possible to propose the transformation

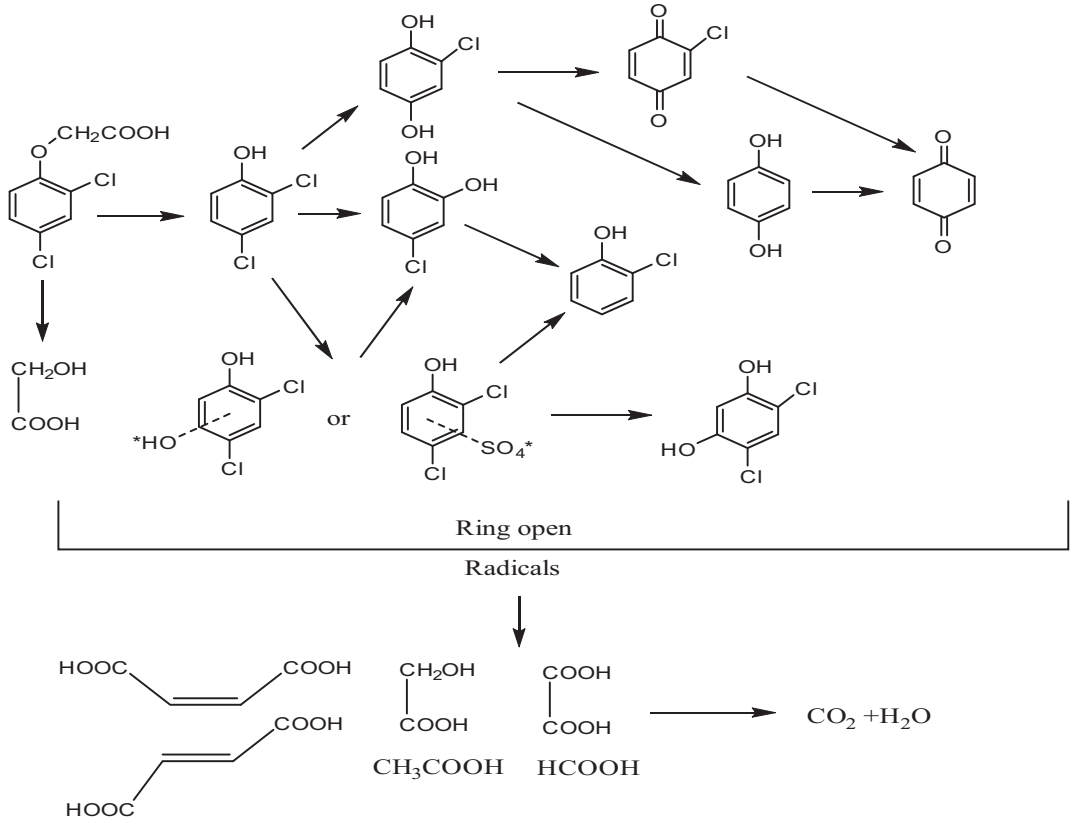

Fig. 20. Possible pathways for photodegradation of 2,4-dichlorophenoxyacetic using CdIn2Se4@Ch.

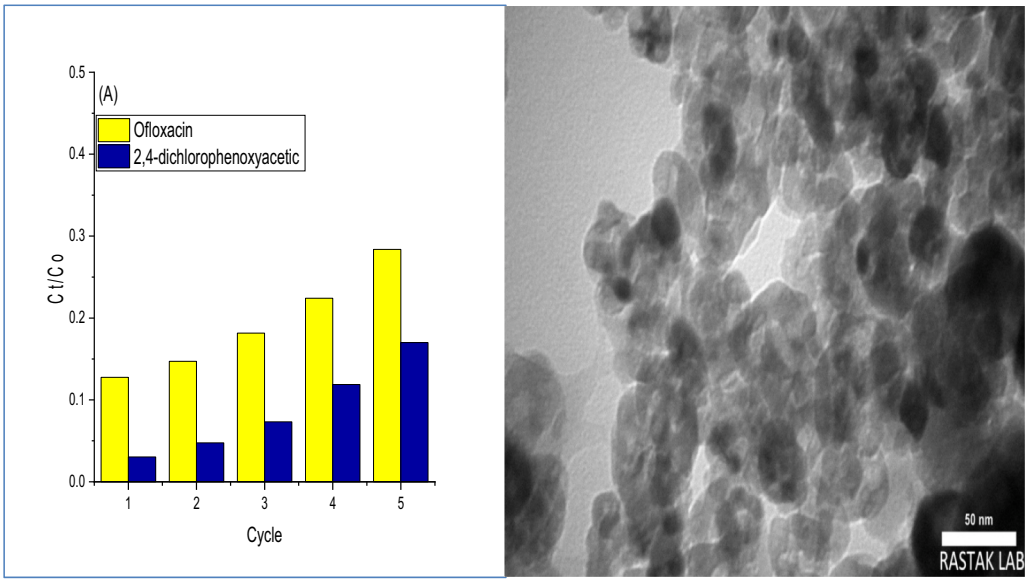

Fig. 21. (A) Reusability of $CdIn_2Se_4$@Ch for the degradation of ofloxacin and 2,4-dichlorophenoxyacetic, (B) TEM images of $CdIn_2Se_4$@Ch after 5 cycle.

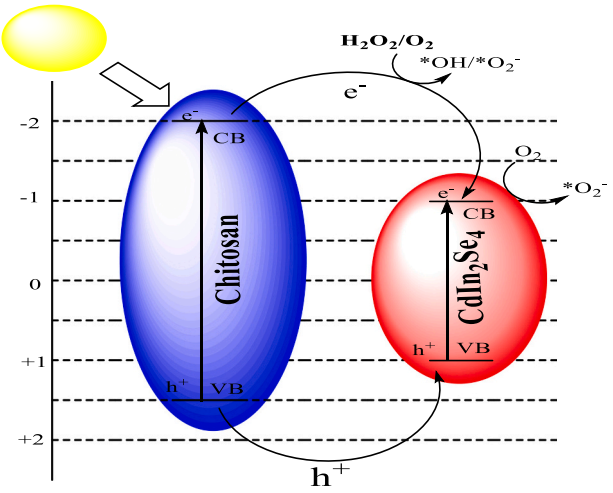

Fig. 22. Schematic representation of the photodegradation mechanism for ofloxacin and 2,4-dichlorophenoxyacetic by synthesized $CdIn_2Se_4$@Ch nanocomposite.

pathways of 2,4-dichlorophenoxyacetic through AOPs (Fig. 19). As depicted in Fig. 20, the activated radicals (OH* and SO4*) primarily targeted the C—O bond in the phenoxy group of 2,4-dichlorophenoxyacetic to break the side chain, resulting in the formation of 2,4-dichlorophenol glycolic acid. Subsequently, the generated glycolic acid could undergo conversion to oxalic acid through the elimination of hydrogen and hydroxyl groups, and finally be transformed into $CO_2 + H_2O$.

4.10. Reusability

The study examined the recyclability of the synthesized CdIn2Se4@chitosan to determine its stability and reusability as shown in Fig. 21a. For each subsequent cycle, the $CdIn_2Se_4$@chitosan photocatalyst needed to be separated by centrifugation, washed with acetone and deionized water multiple times, and then dried at 70 °C for 3 h. The results indicate that the synthesized photocatalyst could be reused up to five times without a significant decrease in performance. However, the alteration of the porous structure of chitosan and the hindrance of surface sites may result in a slight decrease in efficiency. The active separation of charges and support of the chitosan matrix play a significant role in maintaining the stability of $CdIn_2Se_4$@chitosan. It was remarkable to observe that, even after five cycles, the prepared nanocomposite exhibited a high performance with 60 % and 75 % efficiency, demonstrating excellent reusability. Furthermore, the reused photocatalyst was analyzed using TEM after five cycles to assess its stability. The TEM findings revealed that the morphology of the synthesized photocatalyst remained unchanged after 5 cycles, as depicted in Fig. 21b.

4.11. Photodegradation mechanism

Fig. 22 presents a schematic representation of the photodegradation mechanism of ofloxacin and 2,4-dichlorophenoxyacetic acid under sunlight. Upon exposure to sunlight, $CdIn_2Se_4$@chitosan facilitates the excitation of electrons from the valence band to the conduction band, resulting in the formation of holes. Photoluminescence analysis highlights the role of the dopant in scavenging electrons and suppressing recombination between holes and electrons when exposed to sunlight. The photocatalytic capability is significantly enhanced by inhibiting the recombination of electron-hole pairs. The potentials of the conduction band and valence band can be determined using the following equations [69] [108–110]:

$$E_{CB} = X - E^e - 0.5Eg \quad (14)$$

$$E_{VB} = E_{CB} + Eg \quad (15)$$

where X values for CdIn2Se4 and chitosan are 4.97 and 4 respectively. The Eg values for $CdIn_2Se_4$ and chitosan were estimated as 2.1 and 3.4, respectively, through UV–Vis analysis and Tauc plot. As a result, the ECB and EVB values for $CdIn_2Se_4$ were calculated to be −0.77 eV and 1.33 eV, while for chitosan they were found to be −2 eV and 1.5 eV. The energy gap of chitosan encapsulated the edge sites of the CB and VB for $CdIn_2Se_4$, leading to prominent properties characteristic of a type-1 heterojunction. Based on the reactive oxygen species obtained from the scavenger experiment mentioned earlier and the bandgap analysis, the charge transfer mechanism for ofloxacin and 2,4-dichlorophenoxyacetic was calculated. The $CdIn_2Se_4$ and chitosan, due to their effective sunlight capture capabilities, are activated by sunlight to generate electrons and holes in the valence band and conduction band respectively. The calculated values for $*OH/H_2O$ and $*OH/OH^-$ at 1.99 and

Table 3
Photodegradation performance by using different catalyst.

Pollutants	Catalyst	Conc.	Cata. dose (g/L)	Time (min)	Light source	Efficiency (%)	Ref.
	CdS/TiO_2	5	0.45	180	Sunlight	86	[71]
	$Gd_2Ti_2O_7/SiO_2$	20	0.4	90	UV	79	[72]
Ofloxacin	BPQDs/OV-BiOBr	10	1	90	Xe-lamp	98	[73]
	$BaTiO_3/WS_2$	20	1	75	Sunlight	90	[74]
	$CdIn_2Se_4$@Ch	5	0.1	90	Sunlight	86	Our study
	N/TiO_2	40	0.1	180	Sunlight	83	[75]
	Sr/TiO_2	50	1	150	UV	46	[76]
2,4-Dichlorophenoxyacetic acid	Pt/TiO_2	20	0.5	40	UV	91	[77]
	rGO/TiO_2	50	0.2	120	UV	96	[78]
	$CdIn_2Se_4$@Ch	10	0.13	90	Sunlight	98	Our study

2.40 eV/NHE, respectively, indicate that the holes generated in $CdIn_2Se_4$ and chitosan do not readily interact with OH^- or H_2O in the solution, preventing the formation of hydroxyl free radicals which would be ultimately collected in the valence band (VB). Thus, it can be inferred that the holes in the synthesized $CdIn_2Se_4$@chitosan nanocomposite do not lead to the production of hydroxyl free radicals. The potential for chitosan is more positive than that of $CdIn_2Se_4$, while the CB potential for chitosan is more negative than that of $CdIn_2Se_4$ in the heterostructure. As a result, electrons in the CB of chitosan can transfer to the CB of $CdIn_2Se_4$ due to the internal electric field, and holes formed in the VB of chitosan can transfer to the VB of $CdIn_2Se_4$. This type-1 e-h pairs emigration mechanism significantly enhances the separation of e-h pairs at the interface of the heterojunction, despite differences in migration rates between electrons and holes from chitosan to $CdIn_2Se_4$ [70]. The (e-) present on the conduction band of $CdIn_2Se_4$ can combine with O_2, resulting in the formation of superoxide anion $*O_2^-$. This anion then promptly interacts with ofloxacin and 2,4-dichlorophenoxyacetic due to the more negative potential of the conduction band of $CdIn_2Se_4$ compared to $O_2/*O_2^-$.The harmful compounds of ofloxacin and 2,4-dichlorophenoxyacetic can be efficiently oxidized through the vacancies in the $CdIn_2Se_4$ valence band. Additionally, in order to increase the concentration of hydroxyl radicals (*OH), H_2O_2 was introduced into the photodegradation system. H_2O_2 acts as an electron scavenger, interacting with electrons transferred from chitosan conduction band to CdIn2Se4, leading to the production of *OH radicals. The capture of electrons enhances the rate of charge carrier transfer. However, excessive H_2O_2 may consume other ROS and reduce the efficacy of photodegradation for ofloxacin and 2,4-dichlorophenoxyacetic. Therefore, the optimal dose of hydrogen peroxide was determined to ensure accurate concentration for application in the degradation system. Eqs. 16–21 describe the reaction processes under sunlight illumination.

$$H_2O + e^-(CdIn_2Se_4@chitosan) \rightarrow *OH + OH^- \quad (16)$$

$$H_2O_2 + h + (CdIn_2Se_4@chitosan) \rightarrow O2 + 2H + \quad (17)$$

$$H_2O_2 + *O_2^- \rightarrow O_2 + OH^- + *OH \quad (18)$$

$$OH^- + h + (CdIn2Se4@chitosan) \rightarrow *OH \quad (19)$$

$$^*OH + (ofloxacin/2,4\text{-dichlorophenoxyacetic}) \rightarrow degradation\ by\ product + CO_2 + H_2O \quad (20)$$

$$H^+ + (ofloxacin/2,4\text{-dichlorophenoxyacetic}) \rightarrow degradation\ by\ product + CO_2 + H_2O \quad (21)$$

As debated in the comparison the CdIn2Se4@chitosan photocatalyst with different published studies in Table. 3, the ofloxacin and 2,4-dichlorophenoxyacetic were degraded prior, but our prepared photocatalyst appeared high efficiency even at low dosage with sunlight irradiation.

5. Conclusion

This study investigated the photodegradation process of ofloxacin and 2,4-dichlorophenoxyacetic using pristine $CdIn_2Se_4$ and $CdIn_2Se_4$ incorporated with chitosan. The inclusion of chitosan significantly enhanced the speed of photodegradation and mineralization of both ofloxacin and 2,4-dichlorophenoxyacetic compared to using only $CdIn_2Se_4$. It was observed that the degradation of ofloxacin was more favorable in a natural environment, while the degradation of 2,4-dichlorophenoxyacetic was more effective under acidic conditions. The efficacy of photodegradation for ofloxacin and 2,4-dichlorophenoxyacetic acid increased as the dosage of the photocatalyst was raised and the temperature was lowered. Also, the presence of benzoic acid had a significant inhibitory effect on the degradation of pollutants through photodegradation. The quenching studies suggested that both $SO4^{2-}$ and OH* played a role in the degradation of pollutants in the $CdIn_2Se_4$@Ch system, with hydroxyl free radicals potentially being the predominant radical species. Based on scavenger studies and LC-Mass analysis, a potential mechanism for pollutant degradation was proposed. The reusability assessments indicated that the synthesized $CdIn_2Se_4$@Ch maintained its activity even after several cycles.

CRediT authorship contribution statement

Zaid H. Mahmoud: Writing – review & editing, Writing – original draft, Methodology, Investigation, Formal analysis. **Yathrib Ajaj:** Writing – original draft, Writing – review & editing. **Ali M. Hussein:** Writing – original draft, Writing – review & editing. **H.N.K. Al-Salman:** Writing – original draft, Writing – review & editing. **Mohammed Ahmed Mustafa:** Writing – original draft, Writing – review & editing. **Eftikhaar Hasan Kadhum:** Writing – original draft, Writing – review & editing. **Sherzod Abdullaev:** Writing – original draft, Writing – review & editing. **Shahad Abdulhadi Khuder:** Writing – original draft, Writing – review & editing. **Ghadir Kamil Ghadir:** Writing – original draft, Writing – review & editing. **Safaa Mustafa Hameed:** Writing – original draft, Writing – review & editing. **Khursheed Muzammil:** Writing – original draft, Writing – review & editing. **Saiful Islam:** Writing – original draft, Writing – review & editing. **Ehsan Kianfar:** Writing – review & editing, Writing – original draft, Methodology, Investigation,

Formal analysis.

Declaration of competing interest

We wish to confirm that there are no known conflicts of interest associated with this publication and there has been no significant financial support for this work that could have influenced its outcome.

Data availability

All data generated or analyzed during this study are included in this published article.

Acknowledgement

The authors extend their appreciation to the Deanship of Scientific Research at King Khalid University, KSA, for funding this work through a research group program under grant number RGP. 2/556/44.

References

[1] Xue Yang, Tongyuan Yang, Xiaoming Liu, Zhen Cao, Gu Jiarui, Yanlong Wang, Enabling efficient and economical degradation of PCDD/Fs in MSWIFA via catalysis and dechlorination effect of EMR in synergistic thermal treatment, Chemosphere 342 (11) (2023), https://doi.org/10.1016/j.chemosphere.2023.140164.

[2] Zaid H. Mahmoud, Reem Adham AL-Bayati, Anees A. Khadom, The Efficacy of Samarium Loaded Titanium Dioxide (Sm: TiO2) for Enhanced Photocatalytic Removal of Rhodamine B Dye in Natural Sunlight Exposure, J. Mol. Struct. 1253 (2022), https://doi.org/10.1016/j.molstruc.2021.132267.

[3] Xiangbo Feng, Jialing Zeng, Jianru Zhu, Kunli Song, Xinya Zhou, Xuanlin Guo, Chong Xie, Jian-Wen Shi, Gd-modified Mn-Co oxides derived from layered double hydroxides for improved catalytic activity and H2O/SO2 tolerance in NH3-SCR of NOx reaction, J. Colloid Interface Sci. 659 (4) (2024), https://doi.org/10.1016/j.jcis.2024.01.043.

[4] X. Zeng, S. Shu, F. Guo, et al., Photocatalytic degradation of ofloxacin by ZnO combined with persulfate under simulated solar light irradiation: performance, kinetics and degradation pathways, Braz. J. Chem. Eng. 40 (2023) 711–722, https://doi.org/10.1007/s43153-022-00282-y.

[5] Zhe Chen, Tinglin Ma, Zongjun Li, Wenjing Zhu, Lingling Li, Enhanced photocatalytic performance of S-scheme $CdMoO_4$/CdO nanosphere photocatalyst, J. Mater. Sci. Technol. 179 (4) (2024), https://doi.org/10.1016/j.jmst.2023.07.029.

[6] M.S. Peres, M.G. Maniero, J.R. Guimarães, Photocatalytic degradation of ofloxacin and evaluation of the residual antimicrobial activity, Photochem. Photobiol. Sci. 14 (2015) 556–562, https://doi.org/10.1039/c4pp00256c.

[7] Chen Wang, Peng Shi, Chao Guo, Rui Guo, Jiangyuan Qiu, CuCo2O4/CF cathode with bifunctional and dual reaction centers exhibits high RhB degradation in electro-Fenton systems, J. Electroanal. Chem., doi:https://doi.org/10.1016/j.jelechem.2024.118072.

[8] L.M. Carvalho, A.F. Soares-Filho, M.S. Lima, et al., 2,4-Dichlorophenoxyacetic acid (2,4-D) photodegradation on WO3-TiO2-SBA-15 nanostructured composite, Environ. Sci. Pollut. Res. 28 (2021) 7774–7785, https://doi.org/10.1007/s11356-020-11085-4.

[9] N. Orooji, A. Takdastan, R. Jalilzadeh Yengejeh, et al., Photocatalytic degradation of 2,4-dichlorophenoxyacetic acid using Fe3O4@TiO2/Cu2O magnetic nanocomposite stabilized on granular activated carbon from aqueous solution, Res. Chem. Intermed. 46 (2020) 2833–2857, https://doi.org/10.1007/s11164-020-04124-9.

[10] I. Raya, G. Widjaja, Z.H. Mahmood, et al., Kinetic, isotherm, and thermodynamic studies on Cr(VI) adsorption using cellulose acetate/graphene oxide composite nanofibers, Appl. Phys. A Mater. Sci. Process. 128 (2022) 167, https://doi.org/10.1007/s00339-022-05307-4.

[11] Rusul Alabada, Mustafa M. Kadhim, Zainab Sabri Abbas, Ahmed Mahdi Rheima, Usama S. Altimari, Ashour H. Dawood, Zainab Talib Abed, Rusul Saeed Radhi, Asala Salam Jaber, Safa K. Hachim, Farah K. Ali, Zaid H. Mahmoud, Ehsan Kianfar, Investigation of effective parameters in the production of alumina gel through the sol-gel method, Case Studies in Chemical and Environmental Engineering 8 (2023), https://doi.org/10.1016/j.cscee.2023.100405.

[12] Zaid Hamid Mahmoud, Marwa Sabbar Falih, Omaima Emad Khalaf, Mohammed Alwan Farhan, Farah Kefah Ali, Photosynthesis of AgBr doping TiO2 nanoparticles and degradation of reactive red 120 dye, Journal of Advanced Pharmacy Education & Research 8 (4) (2018).

[13] I. Raya, H.H. Kzar, Z.H. Mahmoud, et al., A review of gas sensors based on carbon nanomaterial, Carbon Lett. 32 (2022) 339–364, https://doi.org/10.1007/s42823-021-00276-9.

[14] A. Koltsakidou, M. Antonopoulou, M. Sykiotou, et al., Photo-Fenton and Fenton-like processes for the treatment of the antineoplastic drug 5-fluorouracil under simulated solar radiation, Environ. Sci. Pollut. Res. 24 (2017) 4791–4800, https://doi.org/10.1007/s11356-016-8138-3.

[15] Z.H. Mahmoud, R.A. AL-Bayati, A.A. Khadom, Synthesis and supercapacitor performance of polyaniline-titanium dioxide-samarium oxide (PANI/TiO2-Sm2O3) nanocomposite, Chem. Pap. 76 (2022) 1401–1412, https://doi.org/10.1007/s11696-021-01948-6.

[16] Z.H. Mahmoud, R.A. AL-Bayati, A.A. Khadom, Electron transport in dye-sanitized solar cell with tin-doped titanium dioxide as photoanode materials, J. Mater. Sci. Mater. Electron. 33 (2022) 5009–5023, https://doi.org/10.1007/s10854-021-07690-9.

[17] Mohammed Alwan Farhan, Zaid Hamid Mahmoud, Marwa Sabbar Falih, Synthesis and characterization of TiO2/Au nanocomposite using UV-irradiation method and its photocatalytic activity to degradation of methylene blue, Asian J. Chem. 30 (5) (2018).

[18] Noor Sabah Al-Obaidi, Zainab Esmail Sadeq, Zaid H. Mahmoud, Ahmed Najem Abd, Anfal Salam Al-Mahdawi, Farah K. Ali, Synthesis of chitosan-TiO2 nanocomposite for efficient Cr (VI) removal from contaminated wastewater sorption kinetics, thermodynamics and mechanism, J. Oleo Sci. 72 (3) (2023).

[19] Mohammed Asaad Mahdi, Mohammed A. Farhan, Zaid H. Mahmoud, Ahmed Mahdi Rheima, Zainab Sabri Abbas, Mustafa M. Kadhim, Asala Salam Jaber, Safa K. Hachim, Ahmad Hussain Ismail, Direct sunlight photodegradation of congo red in aqueous solution by TiO2/rGO binary system: Experimental and DFT study, Arab. J. Chem. 16 (8) (2023), https://doi.org/10.1016/j.arabjc.2023.104992.

[20] S. Messina, Y. Rodríguez-Lazcano, J. Campos, et al., Thin films of AgIn5(S/se)8 prepared in a two stage process, J. Mater. Sci. Mater. Electron. 28 (2017) 1812–1818, https://doi.org/10.1007/s10854-016-5730-8.

[21] A.A. Vaipolin, Y.A. Nikolaev, Rud', V.Y., et al., Photosensitive structures based on ZnIn2Se4 single crystals, Semiconductors 37 (2003) 414–416, https://doi.org/10.1134/1.1568460.

[22] D.K. Dhruv, B.H. Patel, N. Agrawal, et al., Synthesis, electrical transport mechanisms and photovoltaic characteristics of p-ZnIn2Se4/n-CdTe thin film heterojunction, J. Mater. Sci. Mater. Electron. 33 (2022) 24003–24015, https://doi.org/10.1007/s10854-022-08755-z.

[23] S. Chander, Advancement in CdIn2Se4/CdTe based photoelectrochemical solar cells, in: S. Ikhmayies (Ed.), Advances in Energy Materials. Advances in Material Research and Technology, Springer, Cham, 2020, https://doi.org/10.1007/978-3-030-50108-2_2.

[24] R.R. Sawant, K.Y. Rajpure, C.H. Bhosale, Determination of CdIn2S4 semiconductor parameters by (photo)electrochemical technique, Phys. B Condens. Matter 393 (1–2) (2007), https://doi.org/10.1016/j.physb.2007.01.009.

[25] Mohammad K. Okla, M. Kalil Rahiman, Mostafa A. Abdel-Maksoud, Ibrahim A. Alaraidh, Abdulrahman A. Alatar, Saud S. Al-amri, Hamada AbdElgawad, S. Mika Sillanpää, Sudheer Khan, Tandem CQDs loaded triple metal oxide interface-reinforced built-in electric field for a wide-spectral-responsive photocatalyst, Colloids Surf. A Physicochem. Eng. Asp. 679 (2023), https://doi.org/10.1016/j.colsurfa.2023.132417.

[26] V. Subhiksha, Mohammad K. Okla, P.R. Sivaranjani, Mostafa A. Abdel-Maksoud, Ibrahim A. Saleh, Hashem A. Abu-Harirah, S. Sudheer Khan, Congregating Ag into γ-Bi2O3 coupled with CoFe2O4 for enhanced visible light photocatalytic degradation of ciprofloxacin, Cr(VI) reduction and genotoxicity studies, Chemosphere Nov (342) (2023) 140181, https://doi.org/10.1016/j.chemosphere.2023.140181.

[27] Ojo Samuel, Asmat Ullah Khan, Mohd Hafiz Dzarfan Othman, Tonni Agustiono Kurniawan, Roziana Kamaludin, Takeshi Matsuura, Aniqa Imtiaz, Ahmad Ilyas Rushdan. Visible light-driven TiO2-WO3@GO photocatalyst with catalytic memory for round-the-clock photocatalytic degradation of oilfield-produced water, Ceram. Int. doi:https://doi.org/10.1016/j.ceramint.2024.02.305.

[28] M. Raaja Rajeshwari, Mohammad K. Okla, S. Kokilavani, Mostafa A. Abdel-Maksoud, Ibrahim A. Saleh, Hashem A. Abu-Harirah, Tareq Nayef AlRamadneh, S. Sudheer Khan, Synergistic visible light assisted photocatalytic degradation of p-chlorophenol and rifampicin from aqueous solution using a novel g-C3N4 quantum dots incorporated α-MoO3 nanohybrid – mechanism, pathway and toxicity studies, Chemosphere 339 (2023) 139529.

[29] Ch. Venkata Reddy, Raghava Reddy Kakarla, Bai Cheolho, Jaesool Shim, Tejraj M. Aminabhavi, Heterostructured 2D/2D ZnIn2S4/g-C3N4 nanohybrids for photocatalytic degradation of antibiotic sulfamethoxazole and photoelectrochemical properties, Environ. Res. 15 (225) (2023) 115585.

[30] V.M. Nikale, S.S. Shinde, A.R. Babar, C.H. Bhosale, K.Y. Rajpure, The n-CdIn2Se4/p-CdTe heterojunction solar cells, Sol. Energy 85 (7) (2011), https://doi.org/10.1016/j.solener.2011.03.014.

[31] Zaid H. Mahmoud, Reem Adham AL-Bayati, Anees A. Khadom, Modified anatase phase of TiO2 by WO3 nanoparticles: structural, morphology and spectral evaluations, Materials Today: Proceedings 61 (2022), https://doi.org/10.1016/j.matpr.2021.09.040.

[32] Y. Wang, W. Li, A. Irini, A novel and quick method to avoid H2O2 interference on COD measurement in Fenton system by Na2SO3 reduction and O2 oxidation, Water Sci. Technol. 68 (2013) 1529–1535.

[33] P. Hayati, et al., Photocatalytic activity of new nanostructures of an ag (i) metal–organic framework (ag-MOF) for the efficient degradation of MCPA and 2, 4-D herbicides under sunlight irradiation, New J. Chem. 45 (2021) 3408–3417.

[34] V. Laokawee, T. Sarakonsri, C. Thanachayanont, Synthesis of CdIn2Se4 and Cu0.5Ag1. 5InSe3 compounds via chemical and solid-state methods, J. Electron. Mater. 43 (2014) 1194–1199, https://doi.org/10.1007/s11664-013-2961-9.

[35] N.E.A. El-Naggar, A.M. Shiha, H. Mahrous, et al., Green synthesis of chitosan nanoparticles, optimization, characterization and antibacterial efficacy against multi drug resistant biofilm-forming Acinetobacter baumannii, Sci. Rep. 12 (2022) 19869, https://doi.org/10.1038/s41598-022-24303-5.

[36] M. Triunfo, E. Tafi, A. Guarnieri, et al., Characterization of chitin and chitosan derived from Hermetia illucens, a further step in a circular economy process, Sci. Rep. 12 (2022) 6613, https://doi.org/10.1038/s41598-022-10423-5.
[37] C.Y. Hsu, A.M. Rheima, M.S. Mohammed, et al., Application of carbon nanotubes and graphene-based Nanoadsorbents in water treatment, BioNanoSci 13 (2023) 1418–1436, https://doi.org/10.1007/s12668-023-01175-1.
[38] E.A. Dalchiele, S. Cattarin, M.M. Musiani, Preparation of CdIn2Se4 thin films by electrodeposition, J. Appl. Electrochem. 28 (1998) 1005–1008, https://doi.org/10.1023/A:1003455803638.
[39] T. Potlog, V. Botnariuc, S. Raevschi, M. Dobromir, D. Luca, XRD and XPS of Cd2SnO4 thin films obtained by spray pyrolysis, in: V. Sontea, I. Tiginyanu (Eds.), 3rd International Conference on Nanotechnologies and Biomedical Engineering. IFMBE Proceedings vol. 55, Springer, Singapore, 2016, https://doi.org/10.1007/978-981-287-736-9_10.
[40] J. Sharma, B.C. Beard, Fundamentals of X-ray photoelectron spectroscopy(XPS) and its applications to explosives and propellants, in: S.N. Bulusu (Ed.), Chemistry and Physics of Energetic Materials. NATO ASI Series vol. 309, Springer, Dordrecht, 1990, https://doi.org/10.1007/978-94-009-2035-4_25.
[41] G.Y. Beak, C.W. Jeon, XPS and Raman study of slope-polished Cu(In,Ga)Se2 thin films, Electron. Mater. Lett. 12 (2016) 399–403, https://doi.org/10.1007/s13391-016-6044-y.
[42] I.W. Almanassra, Y. Zakaria, V. Kochkodan, et al., XPS and material properties of raw and oxidized carbide-derived carbon and their application in antifreeze thermal fluids/nanofluids, J. Therm. Anal. Calorim. 147 (2022) 11787–11803, https://doi.org/10.1007/s10973-022-11419-z.
[43] D. Zhao, P. Zhou, X. Li, et al., Facile and eco-friendly synthesis of chitosan-based mesoporous carbon for adsorbent, J. Porous. Mater. (2024), https://doi.org/10.1007/s10934-023-01541-0.
[44] I.B. Amor, H. Hemmami, S.E. Laouini, et al., Influence of chitosan source and degree of deacetylation on antibacterial activity and adsorption of AZO dye from water, Biomass Convers. Biorefinery (2023), https://doi.org/10.1007/s13399-023-03741-9.
[45] Fengjue Wang, Wenjun Zhang, Han Liu, Ronggen Cao, Meng Chen, Roles of CeO2 in preparing Ce-doped CdIn2S4 with boosted photocatalytic degradation performance for methyl orange and tetracycline hydrochloride, Chemosphere 338 (2023), https://doi.org/10.1016/j.chemosphere.2023.139574.
[46] V.M. Nikale, S.S. Shinde, A.R. Babar, C.H. Bhosale, K.Y. Rajpure, Photoelectrochemical performance of sprayed n-CdIn2Se4 photoanodes, Sol. Energy 85 (2) (2011), https://doi.org/10.1016/j.solener.2010.11.020.
[47] M. Pekdemir, D. Aydin, S. Selçuk Pekdemir, et al., Shape memory polymer-based nanocomposites magnetically enhanced with Fe3O4 nanoparticles, J. Inorg. Organomet. Polym. 33 (2023) 1147–1155, https://doi.org/10.1007/s10904-023-02566-3.
[48] A. Grząbka-Zasadzińska, T. Amietszajew, S. Borysiak, Thermal and mechanical properties of chitosan nanocomposites with cellulose modified in ionic liquids, J. Therm. Anal. Calorim. 130 (2017) 143–154, https://doi.org/10.1007/s10973-017-6295-3.
[49] A. Abuessawy, A. Fouda, A.A.H. Abdel-Rahman, et al., A new modified heterocyclic-magnetite chitosan nanocomposite for efficient alizarin red dye removal: adsorption analysis and antibacterial activity, J. Polym. Environ. (2023), https://doi.org/10.1007/s10924-023-03002-w.
[50] E.M. Abdelrazek, A.M. Elzayat, A.A. Elbana, et al., Physical properties of copper oxide nano-composite incorporated PVP/chitosan blend matrix by casting method, Polym. Bull. (2023), https://doi.org/10.1007/s00289-023-05052-5.
[51] Y. Guo, X. Tong, N. Yang, Photocatalytic and electrocatalytic generation of hydrogen peroxide: principles, Catalyst Design and Performance. Nano-Micro Lett. 15 (2023) 77, https://doi.org/10.1007/s40820-023-01052-2.
[52] X. Deng, Q. Zhang, Q. Zhao, et al., Effects of architectures and H2O2 additions on the photocatalytic performance of hierarchical Cu2O nanostructures, Nanoscale Res. Lett. 10 (2015) 8, https://doi.org/10.1186/s11671-014-0726-x.
[53] M. Farag, S.M. El-Dafrawy, S.M. Hassan, ZnO and C/ZnO catalysts synthesized via plant mediated extracts for photodegradation of crystal violet and methyl orange dyes, J. Inorg. Organomet. Polym. (2023), https://doi.org/10.1007/s10904-023-02811-9.
[54] M.E.D.R. Hassan, M.E.S. Barakat, E.H.E. Yosef, Synthesis and evaluation of core–shell nanocomposites for the photodegradation of liner alkyl-benzene sulfonate water contaminations, Int. J. Environ. Sci. Technol. (2023), https://doi.org/10.1007/s13762-023-05181-4.
[55] S.H. Kim, S.Y. Park, G.E. Kim, et al., Effect of pH and temperature on the biodegradation of oxytetracycline, streptomycin, and validamycin A in soil, Appl. Biol. Chem. 66 (2023) 63, https://doi.org/10.1186/s13765-023-00822-1.
[56] A. Salama, A. Mohamed, N.M. Aboamera, et al., Photocatalytic degradation of organic dyes using composite nanofibers under UV irradiation, Appl. Nanosci. 8 (2018) 155–161, https://doi.org/10.1007/s13204-018-0660-9.
[57] T. Shah, T. Gul, K. Saeed, Photodegradation of bromophenol blue in aqueous medium using graphene nanoplates-supported TiO2, Appl Water Sci 9 (2019) 105, https://doi.org/10.1007/s13201-019-0983-z.
[58] H. Kumari, Suman Sonia, et al., A review on photocatalysis used for wastewater treatment: dye degradation, Water Air Soil Pollut. 234 (2023) 349, https://doi.org/10.1007/s11270-023-06359-9.
[59] R. Avilés-Monreal, H.A. Borbón-Nuñez, M.H. Farías, et al., Photocatalytic activity of Fe3O4–Fe2O3 particles supported on mordenite under visible light exposure for methylene blue degradation, SN Appl. Sci. 5 (2023) 389, https://doi.org/10.1007/s42452-023-05611-5.
[60] S. Abbasi, Studying the destruction of pollutant in the presence of photocatalysts based on MWCNTs with controlled values of TiO2 nanoparticles, Appl Water Sci 13 (2023) 100, https://doi.org/10.1007/s13201-023-01903-8.
[61] S. Abbasi, M. Tahari, M. Imani, Prediction of pollutant removal from aqueous solutions using magnetic photocatalysts, Appl Water Sci 13 (2023) 219, https://doi.org/10.1007/s13201-023-02027-9.
[62] V.T. Lukong, C.N. Chukwuati, K. Ukoba, et al., The role of calcination temperature in the self-cleaning functionality of urea-doped TiO2 prepared through In situ heat-assisted sol–gel synthesis, J. Mater. Eng. Perform. 32 (2023) 11143–11156, https://doi.org/10.1007/s11665-023-08727-2.
[63] E. Assayehegn, A. Solaiappan, Y. Chebudie, et al., Influence of temperature on preparing mesoporous mixed phase N/TiO2 nanocomposite with enhanced solar light photocatalytic activity, Front. Mater. Sci. 13 (2019) 352–366, https://doi.org/10.1007/s11706-019-0481-0.
[64] A. Sharara, M. Samy, M. Mossad, et al., Photodegradation of polyethylene debris in water by sulfur-doped TiO2: system optimization, degradation mechanism, and reusability, Environ. Sci. Pollut. Res. (2023), https://doi.org/10.1007/s11356-023-31460-1.
[65] M.H. Amiri Fard, A. Nasiri, H. Daraei, Green synthesis of AgCoFe2O4@Ch/AC as a recyclable, magnetic nanohybrid heterogeneous catalyst in photodegradation of ceftriaxone from aqueous solutions with effluent bioassay, Appl Water Sci 13 (2023) 220, https://doi.org/10.1007/s13201-023-02026-w.
[66] S.G. Shelar, V.K. Mahajan, S.P. Patil, et al., Effect of doping parameters on photocatalytic degradation of methylene blue using ag doped ZnO nanocatalyst, SN Appl. Sci. 2 (2020) 820, https://doi.org/10.1007/s42452-020-2634-2.
[67] A.M. Saleh, Z. Abd El-Wahab, O.A.M. Ali, et al., Performance of new metal complexes for anionic and cationic dyes photodegradation: construction, spectroscopic studies, optical properties, and DFT calculations, Res. Chem. Intermed. 49 (2023) 3287–3326, https://doi.org/10.1007/s11164-023-05049-9.
[68] N. Khan, I. Khan, N. Zada, et al., Utilization of cross-linked chitosan for cobalt adsorption and its reutilization as a photocatalyst for the photodegradation of methyl violet dye in aqueous medium, Appl Water Sci 12 (2022) 107, https://doi.org/10.1007/s13201-022-01633-3.
[69] S. Asaithambi, P. Sakthivel, M. Karuppaiah, et al., Preparation of SnO2 nanoparticles with addition of co ions for photocatalytic activity of brilliant green dye degradation, J. Electron. Mater. 48 (2019) 2183–2194, https://doi.org/10.1007/s11664-019-07061-5.
[70] L. Pretali, E. Fasani, M. Sturini, Current advances on the photocatalytic degradation of fluoroquinolones: photoreaction mechanism and environmental application, Photochem. Photobiol. Sci. 21 (2022) 899–912, https://doi.org/10.1007/s43630-022-00217-z.
[71] A. Kaur, A. Umar, W.A. Anderson, S.K. Kansal, Facile synthesis of CdS/TiO2 nanocomposite and their catalytic activity for ofloxacin degradation under visible illumination, J. Photochem. Photobiol. A Chem. 360 (2018) 34–43.
[72] W. Zhang, Y. Liu, C. Li, Photocatalytic degradation of ofloxacin on Gd2Ti2O7 supported on quartz spheres, J. Phys. Chem. Solids 118 (2018) 144–149.
[73] X. Li, et al., BiOBr with oxygen vacancies capture 0D black phosphorus quantum dots for high efficient photocatalytic ofloxacin degradation, Appl. Surf. Sci. 593 (2022) 153422.
[74] A. Azli, F. Zakeri, A. Khataee, Y. Orooji, A BaTiO3/WS2 composite for piezophoto- catalytic persulfate activation and ofloxacin degradation, Commun. Chem. 5 (2022) 1–14.
[75] M. Abdennouri, A. Elhalil, M. Farnane, H. Tounsadi, F.Z. Mahjoubi, R. Elmoubarki, M. Sadiq, L. Khamar, A. Galadi, M. Baalala, M. Bensitel, Y. El Hafiane, A. Smith, N. Barka, Photocatalytic degradation of 2,4-D and 2,4-DP herbicides on Pt/TiO2 nanoparticles, J. Saudi Chem. Soc. 19 (2015) 485–493.
[76] R.A. Elsalamony, S.A. Mahmoud, Preparation of nano structured ruthenium doped titania for the photocatalytic degradation of 2-chlorophenol under visible light, Arab. J. Chem. 10 (2) (2017) 194–205, https://doi.org/10.1016/j.arabjc.2012.06.008.
[77] D. Huang, T. Yang, Z. Mo, Q. Guo, S. Quan, C. Luo, L. Liu, Preparation of graphene/TiO2 composite nanomaterials and its photocatalytic performance for the degradation of 2,4-dichloro- phenoxyacetic acid, J. Nanomater. (2016).
[78] E. Kianfar, Protein nanoparticles in drug delivery: animal protein, plant proteins and protein cages, albumin nanoparticles, J Nanobiotechnol 19 (2021) 159, https://doi.org/10.1186/s12951-021-00896-3.
[79] X. Feng, J. Zhu, K. Song, J. Zeng, X. Zhou, X. Guo, J.W. Shi, Insight into the reasons for enhanced NH3-SCR activity and SO2 tolerance of Mn-Co layered oxides, Sep. Purif. Technol. 336 (2024) 126285.
[80] X. Feng, J. Zeng, J. Zhu, K. Song, X. Zhou, X. Guo, J.W. Shi, Gd-modified Mn-Co oxides derived from layered double hydroxides for improved catalytic activity and H2O/SO2 tolerance in NH3-SCR of NOx reaction, J. Colloid Interface Sci. 659 (2024) 1063–1071.
[81] W. Zhu, L. Yang, F. Liu, Z. Si, M. Huo, Z. Li, Z. Chen, Metal Ni nano- particles in-situ anchored on CdS nanowires as effective cocatalyst for boosting the photo-catalytic H2 production and degradation activity, J. Alloys Compd. 973 (2024) 172747.
[82] C. Wang, P. Shi, C. Guo, R. Guo, J. Qiu, CuCo2O4/CF cathode with bifunctional and dual reaction centers exhibits high RhB degradation in electro-Fenton systems, J. Electroanal. Chem. 956 (2024) 118072.
[83] Z. Chen, T. Ma, Z. Li, W. Zhu, L. Li, Enhanced photocatalytic performance of S-scheme CdMoO4/CdO nanosphere photocatalyst, J. Mater. Sci. Technol. 179 (2024) 198–207.
[84] X. Zhao, B. Fan, N. Qiao, R.A. Soomro, R. Zhang, B. Xu, Stabilized Ti3C2Tx-doped 3D vesicle polypyrrole coating for efficient protection toward copper in artificial seawater, Appl. Surf. Sci. 642 (2024) 158639.

[85] T. Jiteshwaran, M.K. Okla, B. Janani, M.A. Abdel-maksoud, Y.A. Alwasel, A. A. Alatar, S.S. Khan, Harnessing iron-rich biochar boosted single crystalline Co2VO4 nano-hexagons: A green photo-Fenton catalyst for rifampicin remediation and byproduct toxicity evaluation, Surfaces and Interfaces 45 (2024) 103828.
[86] Y. Zhang, C. Liu, P. Nian, H. Ma, J. Hou, Y. Zhang, Facile preparation of high-performance hydrochar/TiO2 heterojunction visible light photocatalyst for treating Cr (VI)-polluted water, Colloids Surf. A Physicochem. Eng. Asp. 681 (2024) 132775.
[87] G. Harini, V. Subhiksha, M.K. Okla, M.A. Abdel-maksoud, A.A. AL-Ghamdi, A. A. Alatar, S.S. Khan, Construction of sandwich like RGO/BiVO4/ZSM-5 hybrid heterostructure for the enhanced photocatalytic removal of p-chlorophenol, Surfaces and Interfaces 44 (2024) 103774.
[88] L. Sruthi, M.K. Okla, B. Janani, M.A. Abdel-Maksoud, I.A. Saleh, H.A. Abu-Harirah, S.S. Khan, Construction of rGO-Bi2Sn2O7-NiFe2O4 nanoheterojunction system for the enhanced photodegradation of doxycycline: A brief insight on degradation kinetics and toxicological evaluation on Allium cepa, J. Clean. Prod. 434 (2024) 139936.
[89] F. Zhang, Y. Zhang, G. Zhang, Z. Yang, D.D. Dionysiou, A. Zhu, Exceptional synergistic enhancement of the photocatalytic activity of SnS2 by coupling with polyaniline and N-doped reduced graphene oxide, Appl. Catal. B Environ. 236 (2018) 53–63.
[90] M.K. Okla, M.K. Rahiman, M.A. Abdel-Maksoud, I.A. Alaraidh, A.A. Alatar, S. S. Al-amri, S.S. Khan, Tandem CQDs loaded triple metal oxide interface-reinforced built-in electric field for a wide-spectral-responsive photocatalyst, Colloids Surf. A Physicochem. Eng. Asp. 679 (2023) 132417.
[91] V. Subhiksha, M.K. Okla, P.R. Sivaranjani, M.A. Abdel-Maksoud, I.A. Saleh, H. A. Abu-Harirah, S.S. Khan, Congregating ag into γ-Bi2O3 coupled with CoFe2O4 for enhanced visible light photocatalytic degradation of ciprofloxacin, Cr (VI) reduction and genotoxicity studies, Chemosphere 342 (2023) 140181.
[92] B. Shao, Y. Zhu, J. Hu, Y. Zong, Z. Xie, S. Li, F. Qian, Chemical engineering solution for carbon neutrality in cement industry: tailor a pathway from inevitable CO2 emission into syngas, Chem. Eng. J. 483 (2024) 149098.
[93] Y. Zhang, H. Zhang, J. Yao, Y. Song, W. Li, X. Xuan, Coordination tuning of Fe2+ ions concentration in Fe-doped black phosphorus-carbonized cotton fiber (Fe-BP-CCF) composites to regulate photocatalysis and peroxymonosulfate (PMS) activation towards highly efficient degradation of organic pollutants, Chem. Eng. J. (2024) 149326.
[94] M.R. Rajeshwari, M.K. Okla, S. Kokilavani, M.A. Abdel-Maksoud, I.A. Saleh, H. A. Abu-Harirah, S.S. Khan, Synergistic visible light assisted photocatalytic degradation of p-chlorophenol and rifampicin from aqueous solution using a novel g-C3N4 quantum dots incorporated α-MoO3 nanohybrid–mechanism, pathway and toxicity studies, Chemosphere 339 (2023) 139529.
[95] S. Balasurya, A.M. Elgorban, A.H. Bahkali, M.T. Yassin, R. Balakrishnaraja, R. S. Varma, S.S. Khan, Novel self-propelled CuCr2O4-BiI3O9 nanojets for the efficient photodegradation of organics in wastewater: A non-genotoxic nanomaterial for water treatment, Journal of Water Process Engineering 53 (2023) 103657.
[96] K. Sun, H. Yuan, Y. Yan, H. Qin, L. Sun, L. Tan, W. Shi, Visible-light-response 2D/2D Bi2Fe4O9/ZnIn2S4 van der Waals S-scheme heterojunction with efficient photocatalysis-self-Fenton degradation of antibiotics, Journal of Water Process Engineering 58 (2024) 104803.
[97] M. Swedha, M.K. Okla, M.A. Abdel-Maksoud, S. Kokilavani, K. Kamwilaisak, M. Sillanpää, S.S. Khan, Photo-Fenton system Fe3O4/NiCu2S4 QDs towards bromoxynil and cefixime degradation: A realistic approach, Surfaces and Interfaces 38 (2023) 102764.
[98] B. Harikumar, M.K. Okla, S. Kokilavani, B. Almunqedhi, R. Alshuwaish, M. A. Abdel-Maksoud, S.S. Khan, Insights into oxygen defect enriched and non-metal dopant co modulated Fe3O4 nanospheres embedded WO3 nanorods for ameliorated photo- degradation of doxycycline, Cr (VI) reduction and its genotoxicity, J. Clean. Prod. 398 (2023) 136549.
[99] G. Zhang, T. Ge, Y. Zhang, E. Zhang, H. Ma, J. Hou, Hydrothermal preparation of Nb5+−doped α-Fe2O3 nanorods for efficient visible light-driven photocatalytic reduction of hexavalent chromium, Powder Technol. 436 (2024) 119480.
[100] S. Swetha, M.A. Abdel-Maksoud, M.K. Okla, B. Janani, T.M. Dawoud, M.A. El-Tayeb, S.S. Khan, Triple-mechanism driven Fe-doped nn hetero-architecture of Pr6O11-MoO3 decorated g-C3N4 for doxycycline degradation and bacterial photoinactivation, Chem. Eng. J. 461 (2023) 141806.
[101] P.R. Sivaranjani, A. Syed, A.M. Elgorban, A.H. Bahkali, R. Balakrishnaraja, R. S. Varma, S.S. Khan, Fabrication of ternary nano-heterojunction via hierarchical deposition of α-Fe2O3 and β-La2S3 on cubic CoCr2O4 for enhanced photodegradation of doxycycline, J. Ind. Eng. Chem. 118 (2023) 407–417.
[102] Y.C. Zhang, M. Yang, G. Zhang, D.D. Dionysiou, HNO3-involved one-step low temperature solvothermal synthesis of N-doped TiO2 nanocrystals for efficient photocata- lytic reduction of Cr (VI) in water, Appl. Catal. B Environ. 142 (2013) 249–258.
[103] S. Balasurya, M.K. Okla, H. AbdElgawad, A.A. Al-Ghamdi, M.A. Abdel-Maksoud, S.S. Al-Amri, S.S. Khan, Self-propelled nanojets an interfacial Schottky junctions modulated oxygen vacancies enriched for enhanced photo-Fenton degradation of organic contaminant: improving H2O2 generation, Fe3+/Fe2+ cycle and enhancing plant metabolism, Chemosphere 314 (2023) 137516.
[104] Y. Zhang, F. Zhang, Z. Yang, H. Xue, D.D. Dionysiou, Development of a new efficient visible-light-driven photocatalyst from SnS2 and polyvinyl chloride, J. Catal. 344 (2016) 692–700.
[105] S. Balasurya, M.K. Okla, H. AbdElgawad, A.A. Al-Ghamdi, M.A. Abdel-Maksoud, S.S. Al-Amri, S.S. Khan, Sunlight promoted self-Fenton photodegradation and pathway of doxycycline: interactive effects of nanomaterial on bean plant and its genotoxicity against Allium cepa, Chemosphere 313 (2023) 137286.
[106] S. Kokilavani, A.A. AL-Ghamdi, M.K. Okla, S.A. Al-amri, A.A. Alatar, M.A. Abdel-Maksoud, S.S. Khan, Interfacial engineering of CQDs sensitized NiFe2O4 spheres anchored CoCr2O4/MoO3-x NSs for boosted visible light driven photodegradation of antibiotic, mechanistic insights, and its toxicity assessment, Journal of Water Process Engineering 51 (2023) 103355.
[107] S. Balasurya, A.M. Elgorban, A.H. Bahkali, M.T. Yassin, R. Balakrishnaraja, R. S. Varma, S.S. Khan, Novel self-propelled CuCr2O4-BiI3O9 nanojets for the efficient photodegradation of organics in wastewater: A non-genotoxic nanomaterial for water treatment, Journal of Water Process Engineering 53 (2023) 103657.
[18] T. Ge, Z. Jiang, L. Shen, J. Li, Z. Lu, Y. Zhang, F. Wang, Synthesis and application of Fe3O4/FeWO4 composite as an efficient and magnetically recoverable visible light-driven photocatalyst for the reduction of Cr (VI), Sep. Purif. Technol. 263 (2021) 118401.
[109] B. Janani, R. Balakrishnaraja, A.M. Elgorban, A.H. Bahkali, R.S. Varma, A. Syed, S.S. Khan, Eco-friendly cubic-ZnS coupled Cu7S4 spines on chitosan matrix: unravelling defect-engineered nanoplatform for the photodegradation of p-chlorophenol, J. Environ. Manag. 326 (2023) 116615.
[108] B. Harikumar, S. Kokilavani, S.S. Khan, Magnetically separable N/S doped Fe3O4 embedded on MoO3 nanorods for photodegradation of cefixime, Cr (VI) reduction, and its genotoxicity study, Chem. Eng. J. 446 (2022) 137273.
[109] K. Sun, H. Yuan, Y. Yan, H. Qin, L. Sun, L. Tan, W. Shi, Visible-light-response 2D/2D Bi2Fe4O9/ZnIn2S4 van der Waals S-scheme heterojunction with efficient photocatalysis-self-Fenton degradation of antibiotics, Journal of Water Process Engineering 58 (2024) 104803.
[110] B. Harikumar, S.S. Khan, Hierarchical construction of ZrO2/CaCr2O4/BiOIO3 ternary photocatalyst: Photodegradation of antibiotics, degradation pathway, toxicity assessment, and genotoxicity studies, Chem. Eng. J. 442 (2022) 136107.
[111] A. Mohammadkhani, F. Mohammadkhani, N. Farhadyar, M.S. Sadjadi, Novel nanocomposite zinc phosphate/polyvinyl alcohol/carboxymethyl cellulose: synthesis, characterization and investigation of antibacterial and anticorrosive properties, Case Studies in Chemical and Environmental Engineering 9 (2024) 100591.
[112] Y. Ajaj, H.N.K. Al-Salman, A.M. Hussein, M.K. Jamee, S. Abdullaev, A.A. Omran, Z.H. Mahmoud, Effect and investigating of graphene nanoparticles on mechanical, physical properties of polylactic acid polymer, Case Studies in Chemical and Environmental Engineering 9 (2024) 100612.
[113] A. Mohammadkhani, F. Mohammadkhani, M.S. Sadjadi, N. Farhadyar, M.J. S. Fard, M. Zakani, Preparation and characterization of anticorrosive and antibacterial coatable nanocomposite based on zinc phosphate modified by hydroxy apatite/alginate: investigation of electrochemical impedance spectroscopy (EIS), Case Engineering (2024) 100694.
[114] C.Y. Hsu, Y. Ajaj, G.K. Ghadir, H.M. Al-Tmimi, Z.K. Alani, A.A. Almulla, S. Habibzadeh, Rechargeable batteries for energy storage: A review, e-Prime-Advances in Electrical Engineering, Electronics and Energy (2024) 100510.
[115] Z.H. Mahmoud, Y. Ajaj, G.K. Ghadir, H.M. Al-Tmimi, H.H. Jasim, M. Al-Salih, G. F. Smaisim, Carbon-doped titanium dioxide (TiO2) as Li-ion battery electrode: synthesis, characterization, and performance, Results in Chemistry (2024) 101422.
[116] C.Y. Hsu, H.N.K. Al-Salman, H.H. Hussein, N. Juraev, Z.H. Mahmoud, S.J. Al-Shuwaili, S. Azat, Experimental and theoretical study of improved mesopo- rous titanium dioxide perovskite solar cell: the impact of modification with graphene oxide, Heliyon (2024).
[117] C.Y. Hsu, Z.H. Mahmoud, S. Abdullaev, F.K. Ali, Y.A. Naeem, R.M. Mizher, S. Habibzadeh, Nano titanium oxide (nano-TiO2): a review of synthesis methods, properties, and applications, Case Studies in Chemical and Environmental Engineering (2024) 100626.
[118] E. Kianfar, Comparative studies of nanosheet-based supercapacitors: A review of advances in electrodes materials, Case Studies in Chemical and Environmental Engineering (2023) 100584.
[119] H.N.K. Al-Salman, C.Y. Hsu, Z.N. Jawad, Z.H. Mahmoud, F. Mohammed, A. Saud, E. Kianfar, Graphene oxide-based biosensors for detection of lung cancer: a review, Results in Chemistry (2023) 101300.
[120] C.Y. Hsu, A.M. Rheima, M.S. Mohammed, M.M. Kadhim, S.H. Mohammed, F. H. Abbas, E. Kianfar, Application of carbon nanotubes and graphene-based nanoadsorbents in water treatment, BioNanoScience 13 (4) (2023) 1418–1436.
[121] H.N.K. Al-Salman, M. Sabbar Falih, H.B. Deab, U.S. Altimari, H.G. Shakier, A. H. Dawood, E. Kianfar, A study in analytical chemistry of adsorption of heavy metal ions using chitosan/graphene nanocomposites, Case Studies in Chemical and Environmental Engineering 8 (2023) 100426.
[122] R. Alabada, M.M. Kadhim, Z. Sabri Abbas, A.M. Rheima, U.S. Altimari, A. H. Dawood, E. Kianfar, Investigation of effective parameters in the production of alumina gel through the sol-gel method, Case Studies in Chemical and Environmental Engineering 8 (2023) 100405.
[123] M. Fattahi, C.Y. Hsu, A.O. Ali, Z.H. Mahmoud, N.P. Dang, E. Kianfar, Severe Plastic Deformation: Nanostructured Materials, Metal-Based and Polymer-Based Nano- Composites: A Review, Heliyon, 2023.
[124] C.Y. Hsu, Z.H. Mahmoud, S. Abdullaev, B.A. Mohammed, U.S. Altimari, M. L. Shaghnab, G.F. Smaisim, Nanocomposites based on resole/graphene/carbon fibers: a review study, Case Studies in Chemical and Environmental Engineering (2023) 100535.
[126] E. Darabi, H. Nazarpour-Fard, E. Kianfar, Fast NO2 gas pollutant removal using CNTs/TiO2/CuO/zeolite nanocomposites at the room temperature, Case Studies in Chemical and Environmental Engineering 8 (2023) 100527.

[127] Z. Sabri Abbas, M.M. Kadhim, A. Mahdi Rheima, A.D. Jawad Al-Bayati, Z. Talib Abed, F.M. Dashoor Al-Jaafari, E. Kianfar, Preparing hybrid nanocomposites on the basis of resole/graphene/carbon fibers for investigating mechanical and thermal properties, BioNanoScience 13 (3) (2023) 983–1011.
[128] N. Sabah Ahmed, C.Y. Hsu, Z.H. Mahmoud, H. Sayadi, A graphene oxide/polyaniline nanocomposite biosensor: synthesis, characterization, and electrochemical detection of bilirubin, RSC Adv. 13 (51) (2023) 36280–36292.
[129] M.M. Kadhim, A.M. Rheima, Z.S. Abbas, H.H. Jlood, S.K. Hachim, W.R. Kadhum, Evaluation of a biosensor-based graphene oxide-DNA nanohybrid for lung cancer, RSC Adv. 13 (4) (2023) 2487–2500.
[130] F. Kianfar, E. Kianfar, Synthesis of isophthalic acid/aluminum nitrate thin film nanocomposite membrane for hard water softening, J. Inorg. Organomet. Polym. Mater. 29 (2019) 2176–2185.